AUTOPHAGY
2016, VOL. 12, NO. 9, 1614–1630
http://dx.doi.org/10.1080/15548627.2016.1192752

Taylor & Francis
Taylor & Francis Group

BASIC RESEARCH PAPER

MARCH2 regulates autophagy by promoting CFTR ubiquitination and degradation and PIK3CA-AKT-MTOR signaling

Dan Xia[a,b,c], Liujing Qu[a,b,c], Ge Li[a,b,c], Beiqi Hongdu[a,b,c], Chentong Xu[a,b,c], Xin Lin[a,b,c], Yaxin Lou[d], Qihua He[d], Dalong Ma[a,b,c], and Yingyu Chen[a,b,c]

[a]Department of Immunology, Peking University School of Basic Medical Sciences, Beijing, China; [b]Key Laboratory of Medical Immunology, Ministry of Health, Peking University Health Sciences Center, Beijing, China; [c]Center for Human Disease Genomics, Peking University, Beijing, China; [d]Medical and Healthy Analytical Center, Peking University, Beijing, China

ABSTRACT

MARCH2 (membrane-associated RING-CH protein 2), an E3 ubiquitin ligase, is mainly associated with the vesicle trafficking. In the present study, for the first time, we demonstrated that MARCH2 negatively regulates autophagy. Our data indicated that overexpression of MARCH2 impaired autophagy, as evidenced by attenuated levels of LC3B-II and impaired degradation of endogenous and exogenous autophagic substrates. By contrast, loss of *MARCH2* expression had the opposite effects. In vivo experiments demonstrate that *MARCH2* knockout mediated autophagy results in an inhibition of tumorigenicity. Further investigation revealed that the induction of autophagy by *MARCH2* deficiency was mediated through the PIK3CA-AKT-MTOR signaling pathway. Additionally, we found that MARCH2 interacts with CFTR (cystic fibrosis transmembrane conductance regulator), promotes the ubiquitination and degradation of CFTR, and inhibits CFTR-mediated autophagy in tumor cells. The functional PDZ domain of MARCH2 is required for the association with CFTR. Thus, our study identified a novel negative regulator of autophagy and suggested that the physical and functional connection between the MARCH2 and CFTR in different conditions will be elucidated in the further experiments.

ARTICLE HISTORY
Received 31 July 2015
Revised 12 May 2016
Accepted 18 May 2016

KEYWORDS
autophagy; CFTR; MARCH2; MTOR; protein degradation

Introduction

Autophagy is a major cellular degradation pathway in which cytosolic long-lived proteins and organelles are captured into autophagosomes and delivered to lysosomes, where the sequestered cargo is degraded and recycled.[1] Autophagy exists at a low level in basal physiological conditions, but is induced to a high level upon starvation or other stress conditions.[2] Its high capacity means that autophagy plays a key role in preserving homeostasis and protein quality control.

Upon conventional autophagy activation, MTORC1 dissociates from the ULK1 complex, leading to ULK1 dephosphorylation and activation. ULK1 then phosphorylates AMBRA1, releasing it and the PIK3C3-BECN1 complex from the cytoskeleton, enabling the PIK3C3-BECN1 complex to relocate into the ER (endoplasmic reticulum), which marks the initiation of an autophagosome. Next, ATG9 is recruited to carry lipids for membrane elongation, which serves as a platform for recruiting effectors to the phagophore. Two ubiquitin-like conjugation systems mediate phagophore shaping, expansion and sealing. First, assisted by E1-like enzyme ATG7 and E2-like enzyme ATG10, ATG12 conjugates with ATG5, and together with ATG16L1, forms the ATG12–ATG5-ATG16L1 complex. Second, LC3 (microtubule-associated protein 1 light chain 3) is cleaved by ATG4 to produce LC3-I, which links to PE to produce lipidated and phagophore/autophagosome-localized LC3-II.[3] LC3-II is ever present during the formation and maturation of autophagosomes; therefore, LC3-II is considered as a marker of autophagy.[4-8]

MARCH2 (membrane associated ring-CH-type finger 2) is a member of the MARCH family, which includes at least 9 members currently. MARCH2 is characterized by a RING-CH finger (N terminus), 2 transmembrane spans (middle) and a PDZ domain binding motif (C terminus).[9] The RING-CH finger is a C4HC3-type double Zn^{2+}-binding domain, which has E3 ubiquitin ligase activity. MARCH2 was identified for the first time as a member of a novel transmembrane ubiquitin ligase family probably associated with viral immune evasion proteins.[10] It interacts with STX6 (syntaxin 6) and participates in the transportation between the *trans*-Golgi network (TGN) and early endosomes or recycling endosomes. It mainly functions in vesicle trafficking.[11] As an E3 ubiquitin ligase, MARCH2 can ubquitinate several substrates, such as DLG1,[12] ADRB2/β2AR[13] and CFTR.[14] To date, the role of MARCH2 in autophagy remains unclear.

In the present study, for the first time, we reported a correlation between MARCH2 and autophagy. A series of experiments proved that MARCH2 is a negative regulator of autophagy. The potential molecular mechanism of MARCH2-mediated

CONTACT Yingyu Chen yingyu_chen@bjmu.edu.cn Department of Immunology, Peking University School of Basic Medical Sciences, 38 Xueyuan Road, Beijing, 100191, P.R. China
Supplemental data for this article can be accessed on the publisher's website.

autophagy might promote the ubiquitination and degradation of CFTR. Simultaneously, PIK3CA-AKT-MTOR signaling is also associated with the autophagy regulation triggered by MARCH2.

Results

MARCH2 overexpression impairs autophagosome formation

We previously established a screening platform for novel human autophagy-related genes, based on an automated fluorescence microscopy system,[15] and have identified several genes linked to cell autophagy, including *TM9SF1*,[15] *EMC6*,[16] *TMEM208*,[17] *PHF23*[18] and *MARCH2*. Here, we analyzed the effects of *MARCH2* on autophagy regulation systematically.

We first detected the expression and intracellular distribution of MARCH2 during the autophagic process. Data obtained from western blotting showed that the expression of MARCH2 was downregulated in HeLa cells treated with EBSS or rapamycin in time-dependent manner (Fig. S1A). Similar results were observed in glucose-starved cells (Fig. S1B, lane 1 to 4), which indicates that MARCH2 was degraded in the process of autophagy. Therefore, E64d plus pepstatin A (inhibitors of autophagic substrate degradation) were used to further confirm whether MARCH2 was degraded via autophagy. As shown in Figure S1B (lane 5 to 8), treatment of E64d plus pepstatin A could increase the levels of MARCH2 in glucose-starved HeLa cells. We also found that MG132 (a proteasome inhibitor) reduced the degradation of MARCH2 protein in glucose-starved HeLa cells (Fig. S1B, lane 9 to 12). These results indicated that the degradation of MARCH2 was due to both autophagy and the proteasome. Consistent with this observation, immunofluorescence and confocal microscopy observations indicated that the fluorescence signals of MARCH2 in plasma and cytoplasm were downregulated in HeLa cells treated with EBSS (Fig. S1C), indicating that the intracellular distribution of MARCH2 should be affected by autophagy-inducing conditions.

Next we analyzed the phenotype of autophagy. In MARCH2-overexpressing HeLa cells, the steady-state levels of endogenous LC3B-II protein decreased compared with the vector control (Fig. 1A and B, lane 2 vs. lane 1). This decrease in LC3B-II potentially resulted from a decrease in autophagosome formation or an increase of autophagosome degradation.[5,8] To distinguish these 2 possibilities, bafilomycin A_1 ($BafA_1$) was used. $BafA_1$ prevents the fusion between autophagosomes and lysosomes by inhibiting the vacuolar-type H^+-translocating ATPase. As shown in Figure 1A and B, lane 4 vs. lane 3, compared with empty vector-transfected cells, the LC3B-II accumulation in MARCH2-overexpressing cells was still weaker in the presence of $BafA_1$. This indicated that decreased LC3B lipidation (as it is correlated to LC3B-II levels) driven by MARCH2 overexpression, resulted from decreased autophagosome formation. Furthermore, MARCH2 overexpression attenuated LC3B lipidation in rapamycin-treated HeLa cells, with or without $BafA_1$ (Fig. 1A and B, lane 6 vs. lane 5, lane 8 vs. lane 7), which suggested that MARCH2 overexpression ablated autophagosome formation both in normal and stress conditions. Similar results were acquired in U2OS cells (Fig. 1A and B, lane 9 to lane 16). Consistent with the results of western blotting, we monitored GFP-LC3B puncta per cell in stably transfected GFP-LC3B HeLa cells. Compared with the control group, MARCH2 overexpression reduced the GFP-LC3B puncta distribution in the presence or absence of $BafA_1$ (Fig. 1C and D). At the same time, MARCH2 overexpression also reduced RAPA-induced GFP-LC3B dots in HeLa cells (Fig. 1C and D). The distribution of endogenous LC3B dots was similar to that of GFP-LC3B in MARCH2-overexpressing HeLa cells (Fig. S1D and E). Additionally, MARCH2 overexpression also attenuated EBSS-induced LC3B lipidation (data not shown).

Transmission electron microscopy (TEM) analysis was performed to examine the ultrastructure of autophagic structures in MARCH2-overexpressing HeLa cells treated with $BafA_1$. The results revealed that MARCH2 overexpression resulted in decreased autophagosome- or autolysosome-like structures, compared with the vector-transfected cells (Fig. 1E and F). Taken together, these results demonstrated that MARCH2 overexpression impairs the synthesis of autophagosomes.

During autophagy, the GFP-LC3B protein is delivered to lysosomes, in which the GFP moiety is cleaved and remains relatively stable, while LC3B is rapidly degraded. Thus, the level of free GFP corresponds to the autophagic flux.[8] In stably transfected GFP-LC3B HeLa cells, a weaker free GFP band was observed in MARCH2-overexpressing cells than in control cells (Fig. 1G and H). This treatment also resulted in an increase in the endogenous autophagy substrate SQSTM1[8,19] (Fig. 1G and H, upper panel). Simultaneously, MARCH2 overexpression upregulated exogenously expressed polyQ80 aggregates (Fig. 1I), indicating that MARCH2 impairs the clearance of autophagic substrates.

Knockdown of MARCH2 *increases the complete autophagic flux*

To determine the physiological effect of MARCH2 on the regulation of autophagy, experiments were conducted in *MARCH2*-depleted cells. Using RT-PCR and western blotting, an effective siRNA against *MARCH2* (*siMARCH2*) was identified (Fig. S2A). Data from repeated experiments showed that depletion of *MARCH2* greatly elevated the levels of endogenous LC3B-II (Fig. 2A and B, lane 2 vs. lane 1), compared with *siControl*-transfected cells. $BafA_1$ treatment caused a further increase in LC3B conversion in *MARCH2*-silenced cells (Fig. 2A and B, lane 4 vs. lane 3), which indicated that *MARCH2* deficiency increased the formation of autophagosomes. Additionally, *MARCH2* silencing promoted RAPA-induced lipidation of LC3B, with or without $BafA_1$ (Fig. 2A and B, lane 6 vs. lane 5, lane 8 vs. lane 7). These data indicated that knockdown of *MARCH2* facilitated autophagosome synthesis in normal or stress conditions. Similar results were obtained in U2OS cells (Fig. 2A and B, lane 9 to lane 16). In line with these results, *MARCH2* knockdown remarkably elevated GFP-LC3B dots per cell compared with the *siControl* group, with or without $BafA_1$ (Fig. S2B and C). Furthermore, TEM observation suggested that *MARCH2* knockdown cells treated with $BafA_1$ displayed more autophagosome- or autolysosome-like structures than in *siControl*-transfected cells (Fig. 2C and D). To further prove the function of MARCH2, a *MARCH2* knockout cell line was established by CRISPR-Cas9-mediated genome editing[20,21] in HCT166 cells. As expected, CRISPR-Cas9-mediated knockout (KO) of *MARCH2* led to an absence of MARCH2 protein

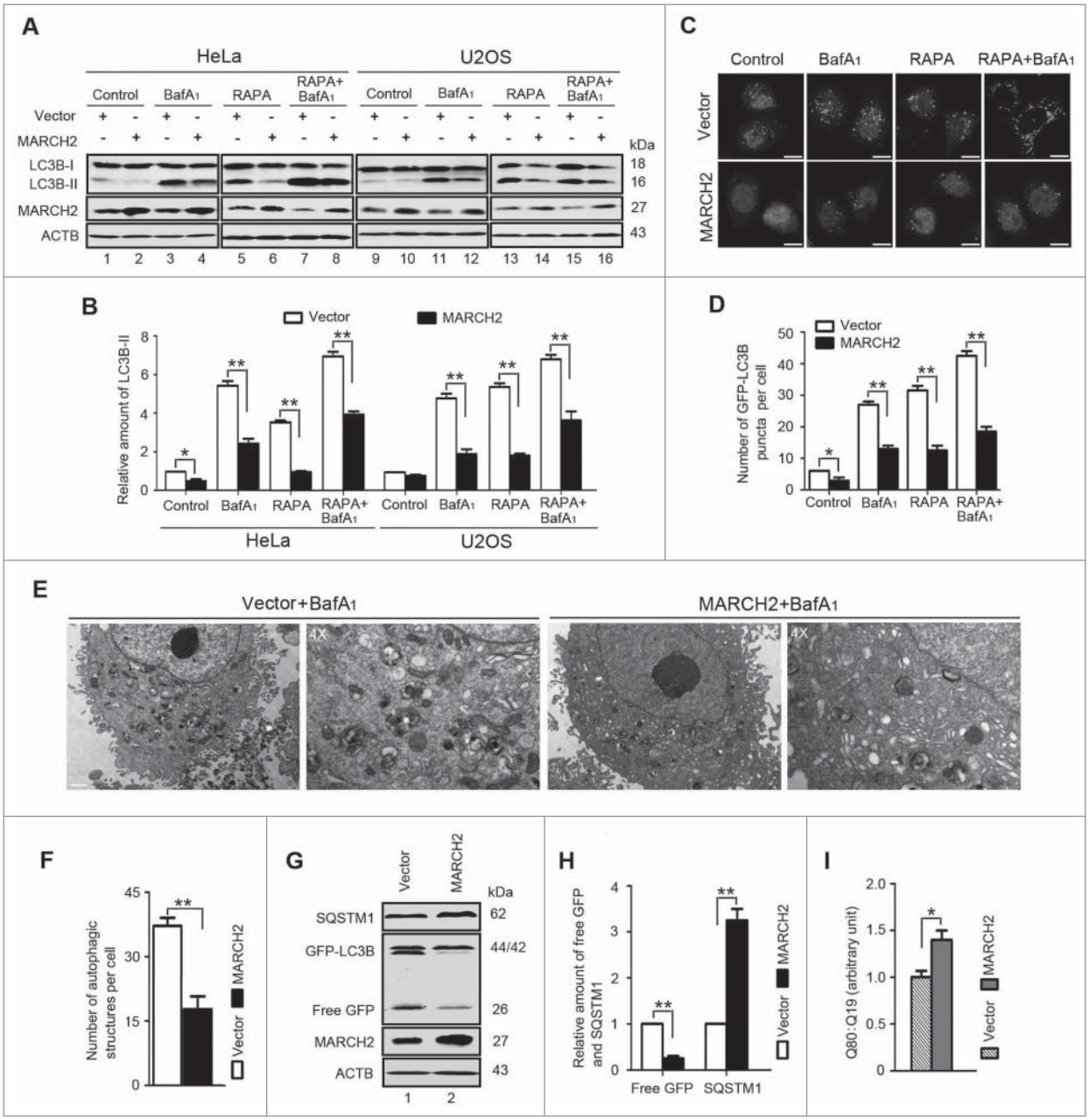

Figure 1. MARCH2 overexpression impairs autophagosome formation. (A) HeLa and U2OS cells were transfected with empty vector (Vector) or the MARCH2-MYC (MARCH2) plasmid for 24 h, and treated with $BafA_1$ (10 nM) and/or rapamycin (RAPA, 5 μM) for the last 6 h. The levels of LC3B-II were measured by western blotting. (B) Quantification of LC3B-II levels relative to ACTB in cells treated as in (A). Average value in vector-transfected cells without $BafA_1$ was normalized as 1. Data are means ± SD of results from 3 experiments. (C) Representative confocal microscopy images of GFP-LC3B distribution obtained from Hela cells transfected with the indicated plasmids and treated as in (A). Scale bar: 25 μm. (D) Quantification of GFP-LC3B puncta per cell treated as in (C). Data are means ± SD of at least 50 cells scored. (E) HeLa cells were transfected with vector or the MARCH2-MYC plasmid for 24 h, and treated with BafA1 (10 nM) for the last 2 h. Cells were then harvested for the TEM analysis. Scale bar: 25 μm. (F) Quantification of autophagic structures per cell treated as in (E). Data are means ± SD of at least 20 cells scored. (G) HeLa cells stably expressing GFP-LC3B were transfected with vector or the MARCH2-MYC plasmid for 24 h. Levels of SQSTM1 and free GFP were analyzed by western blotting. (H) Quantification of amounts of free GFP or SQSTM1 protein relative to ACTB in cells treated as in (G). The average value in Vector-transfected cells was normalized as 1. Data are means ± SD of results from 3 experiments. (I) Hela cells were cotransfected with polyQ80-luciferase (or polyQ19-luciferase) and vector or the MARCH2-MYC plasmids for 24 h. PolyQ80 luciferase:polyQ19 luciferase ratios were analyzed using the Dual Luciferase Reporter System. The average value in vector-transfected cells was normalized as 1. Data are means ± SD of results from 3 experiments. *, $P < 0.05$; **, $P < 0.01$.

(Fig. 2E, lane 2 vs. lane 1). Simultaneously, knockout of *MARCH2* in HCT116 cells also resulted in an accumulation of LC3B-II in the presence or absence of $BafA_1$ (Fig. 2E and F, lane 2 vs. lane 1, lane 5 vs. lane 4; Fig. S2D to G). These results are concordant with those of *siMARCH2* treatment.

In addition to the LC3B expression, autophagosomes had been identified by SQSTM1, ubiquitin, WIPI2,[22-24] ATG16L1[24] and STX17 (syntaxin 17).[25,26] When autophagy is activated, WIPI2 is recruited to early autophagosomal structures along with ATG16L1 and ULK1 and is required for the formation of LC3-positive autophagosomes.[23] STX17 localizes to the outer membrane of completed autophagosomes but not to the phagophore.[25] It targets to autophagosomes for fusion with endosomes/lysosomes.[26] Further studies suggested that knockdown of *MARCH2* indeed increased the colocalization of GFP-LC3B together with SQSTM1, ubiquitin, WIPI2, ATG16L1 or STX17,

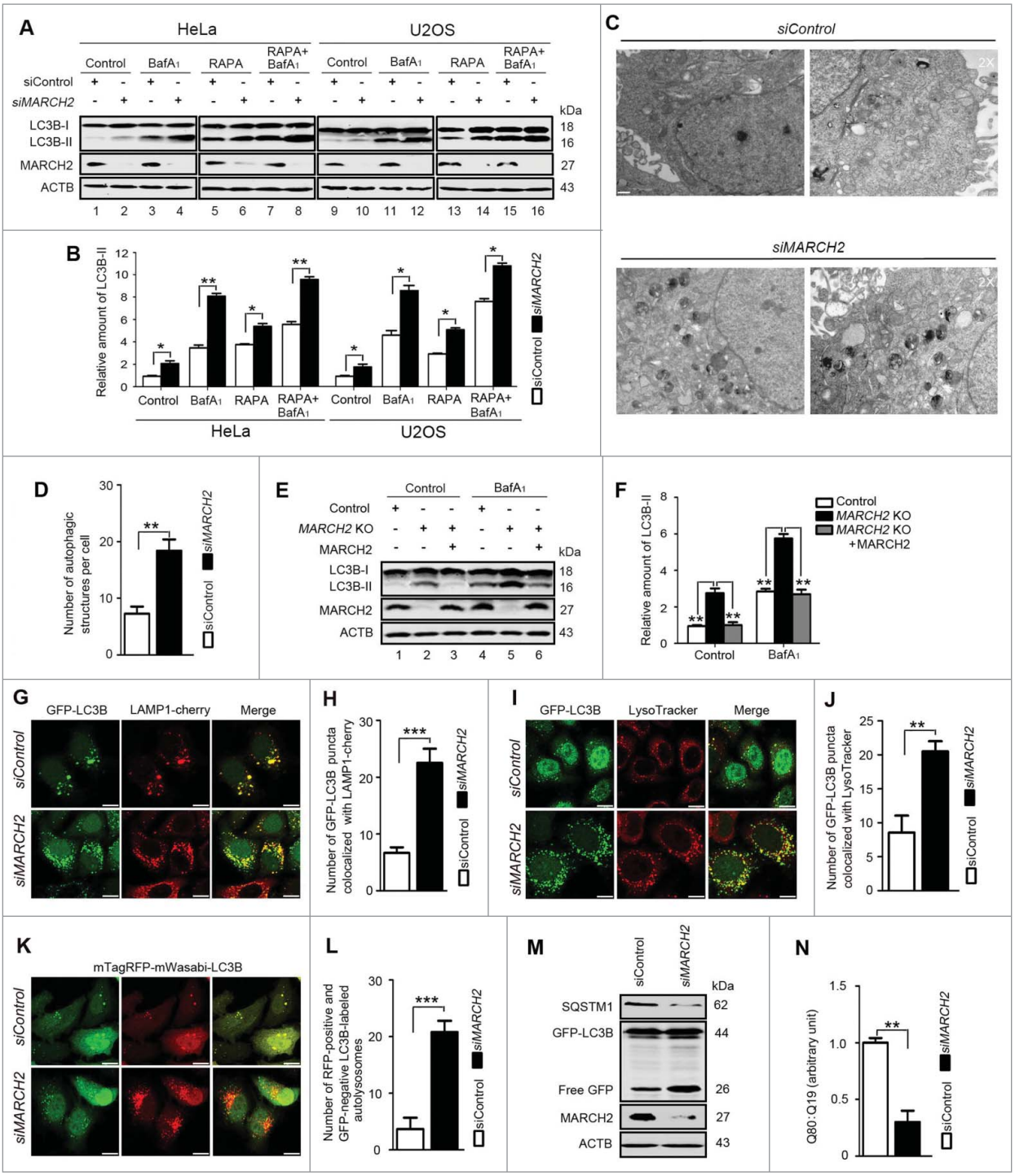

Figure 2. Loss of *MARCH2* increases complete autophagic flux. (A) HeLa and U2OS cells transfected with *siControl* or *siMARCH2* for 48 h and treated with BafA1 (10 nM) and/or RAPA (5 μM) for the last 6 h. The levels of LC3B-II were detected by western blot. (B) Quantification of amounts of LC3B-II relative to ACTB in cells treated as in (A). Average value in *siControl*-transfected cells without $BafA_1$ was normalized as 1. Data are means $\pm$ SD of results from 3 experiments. (C) TEM analysis of HeLa cells transfected with *siControl* or *siMARCH2* for 48 h, and treated with BafA1 (10 nM) for the last 6 h. Scale bar: 1 μm. (D) Quantification of autophagic structures per cell treated as in (E). Data are means $\pm$ SD of at least 20 cells scored. (E) Western blotting analysis of endogenous LC3B-II levels in control HCT116 cells, *MARCH2* KO HCT116 cells alone or *MARCH2* KO HCT116 cells transfected with the MARCH2 plasmid for 24 h, then treated with or without $BafA_1$(10 nM) for the last 6 h. (F) Quantification of endogenous LC3B-II levels relative to ACTB in cells treated as in (C). The average value in control cells without $BafA_1$ was normalized as 1. Data are means $\pm$ SD of results from 3 experiments. (G and I) Colocalization of GFP-LC3B with LAMP1-cherry or LysoTracker Red obtained from stable GFP-LC3B HeLa cells transfected with *siControl* or *siMARCH2* for 48 h, and then observed by confocal microscopy. Scale bar: 25 μm. (H and J) Quantification of number of GFP-LC3B puncta colocalized with LAMP1-cherry or LysoTracker Red per cell. Data are means $\pm$ SD of at least 50 cells scored. (K) Representative confocal microscopy images of mTagRFP-mWasabi-LC3B distribution in HeLa cells cotransfected with mTagRFP-mWasabi-LC3B and *siControl* or *siMARCH2*, and cultured for 48 h. Scale bar: 25 μm. (L) Quantification of number of RFP-positive and GFP-negative LC3B-labeled autolysosomes per cell treated as in (K). Data are means $\pm$ SD of at least 50 cells scored. (M) HeLa cells stably expressing GFP-LC3B were transfected with *siControl* or *siMARCH2* for 48 h. Levels of SQSTM1 and free GFP were analyzed by western blotting. (N) HeLa cells were cotransfected with polyQ80-luciferase (or polyQ19-luciferase) and the indicated siRNAs for 48 h. PolyQ80-luciferase: polyQ19-luciferase ratios were analyzed using the Dual Luciferase Reporter System. The average value in *siControl*-transfected cells was normalized as 1. Data are means $\pm$ SD of results from 3 experiments. *, $P < 0.05$, **; $P < 0.01$; ***, $P < 0.001$.

respectively (Figure S3A to L). Collectively, these results indicated that *MARCH2* deficiency promoted autophagosome formation.

Next, the specific effects of *MARCH2* depletion were assessed in a recovery experiment. As shown in Figure 2E and F, increased LC3B conversion in *MARCH2* KO HCT116 cells was significantly decreased after transfection with the MARCH2 plasmid, with or without $BafA_1$ (Fig. 2E and F, lane 3 vs. lane 2, lane 6 vs lane 5), implying the specific effects of *MARCH2* ablation- modulated autophagy. Consistent with these observations, the LC3B puncta in *MARCH2*-knockout cells plus the MARCH2 overexpression were reduced compared with *MARCH2* KO alone (Fig. S2H and I). Overall, our results suggested that MARCH2 negatively regulates cell autophagy.

We then monitored whether *MARCH2* deficiency increased autophagic flux. In view of the fact that MARCH2 localized to lysosomes,[9] we first analyzed the effects of MARCH2 on lysosomal function. Western blotting revealed that *MARCH2* silencing did not influence the maturation of CTSB or CTSD (Fig. S4A), which indicated that *MARCH2* deficiency failed to affect lysosomal activity. We further detected the maturation of autophagosomes and substrate degradation in *MARCH2*-silenced cells. Autophagosome maturation involves a series of fusions with late endosomes and lysosomes. Confocal microscopy proved that the number of GFP-LC3B puncta colocalized with LAMP1-Cherry was significantly increased in *siMARCH2*-transfected cells compared with that in the *siControl* group (Fig. 2G and H). Simultaneously, the same treatment caused more GFP-LC3B puncta to fuse with LysoTracker Red-labeled lysosomes (Fig. 2I and J). Furthermore, the mTagRFP-mWasabi-LC3B reporter was also used to evaluate the maturation of autophagosomes in *MARCH2* knockdown cells.[27] The data showed that the conversion of mTagRFP-positive and mWasabi-negative LC3B puncta (which have no mWasabi signal, or much weaker relative to mTagRFP) was markedly increased in *MARCH2*-depleted cells compared with *siControl*-transfected cells (Fig. 2K and L). Results from flow cytometry showed that the percentage of $mTagRFP^{High}$ $mWasabi^{Low}$ cells was significantly increased in cells transfected with *siMARCH2*, compared with control cells (Fig. S4B and C). Consistent with these results, in stably transfected GFP-LC3B HeLa cells, stronger free GFP and weaker SQSTM1 bands were observed in *MARCH2*-silenced cells than in control cells (Fig. 2M). This treatment also resulted in a reduction in polyQ80 aggregates (Fig. 2N), indicating that *MARCH2* silencing enhanced autophagic substrate clearance. Collectively, these data supported the view that *MARCH2* deficiency promoted autophagosome entry into lysosomes and degradation.

MARCH2 *knockdown-mediated autophagy acts upstream of ULK1 and the PIK3C3-BECN1 complex*

We next determined at which step the autophagosome formation is increased in the *MARCH2* knockdown cells. At this point, several key ATG molecules, including ATG7, *ATG5, ATG16L1, PIK3C3, BECN1* and *ULK1* were silenced in *MARCH2* knockdown cells and the effects were analyzed. Western blotting showed that *ATG7* knockdown reversed the accumulation of LC3B-II induced by *siMARCH2*, with or without $BafA_1$ treatment (Fig. 3A and B, lane 4 vs. lane 2, lane 8 vs. lane 6). Likewise, knockdown of *ATG5* or *ATG16L1* also blocked the LC3B conversion induced by *siMARCH2* (Fig. 3C–F, lane 4 vs. lane 2, lane 8 vs. lane 6). These data implied that the activity of ATG7, ATG5 and ATG16L1 was required for *MARCH2* silencing-induced autophagy.

3-methyladenine (3-MA), a PIK3C3 inhibitor, was used to indicate whether MARCH2 acts upstream or downstream of the class III phosphatidylinositol 3-kinase complex. As shown in Figure S5A and B, lane 6 vs. lane 4, 3-MA decreased the accumulation of LC3B-II induced by *siMARCH2*. Other PIK3C3 inhibitors, such as wortmannin (WM) and LY294002, also reversed the LC3B lipidation induced by *siMARCH2* (Fig. S5A, lane 8 vs. lane 4, lane 10 vs. lane 4). We then performed the experiments in *BECN1* or *PIK3C3/VPS34*-silenced cells. As showed in Figure 3G to J, *BECN1* or *PIK3C3* deficiency blocked the increases of LC3B-II induced by *siMARCH2* treatment (Fig. 3G–J, lane 4 vs. lane 2, lane 8 vs. lane 6). Similarly, *ULK1* silencing also prevented the LC3B lipidation induced by *siMARCH2* treatment (Fig. 3K and L, lane 4 vs. lane 2, lane 8 vs. lane 6). These data revealed that *MARCH2* knockdown promotes autophagosome formation through the classic autophagic pathway, and that MARCH2 might act upstream of ULK1 and the PIK3C3-BECN1 complex.

PIK3CA-AKT-MTOR signaling is involved with MARCH2-*ablation-triggered autophagy*

Next, we investigated the signaling involved in the autophagy-stimulative effect in *MARCH2*-silenced cells. MTOR (mechanistic target of rapamycin [serine/threonine kinase]) is a key regulator in autophagy induction in response to diverse stimuli, including nutrient deprivation and stress. Its activity is inversely correlated with autophagy induction. Thus, we assessed whether the autophagy effect in *MARCH2* knockdown cells is a result of aberrant MTOR signaling. Experiments showed that the phosphorylation levels of MTOR at Ser2448 (activation site) and RPS6KB1 (a substrate of MTOR) were decreased in *siMARCH2*-treated cells (Fig. 4A). A similar downregulation in phosphorylated RPS6 and EIF4EBP1, other downstream effectors of the MTOR, was also observed in *siMARCH2*-depleted cells (Fig. 4A). These results supported the hypothesis that a decrease of MTOR activity contributes to the *siMARCH2*-induced autophagy.

Activation of PIK3CA results in phosphorylation of phosphatidylinositol (PtdIns)-4, 5-bisphosphate ($PtdIns[4,5]P_2$) to form $PtdIns(3,4,5)P_3$. Subsequently, $PtdIns(3,4,5)P_3$ recruits downstream effector proteins, such as the serine/threonine kinase AKT. Once activated, AKT-mediated phosphorylation of TSC2 inhibits the TSC1-TSC2 complex function, and thus activates MTOR signaling.[8,28,29] Therefore, further experiments were performed to determine the influence of *MARCH2* deletion on the PIK3CA-AKT pathway. As shown in Figure 4A, there was a significant decrease in the phosphorylation of PIK3R1/p85, indicating the inhibition of PIK3R1 activity. Thus the catalytic activity of PIK3CA was decreased. Simultaneously, the downregulated phosphorylation of AKT was observed in the *siMARCH2*-treated cells (Fig. 4A). Importantly, we observed that the basal phosphorylation levels of TSC2 were

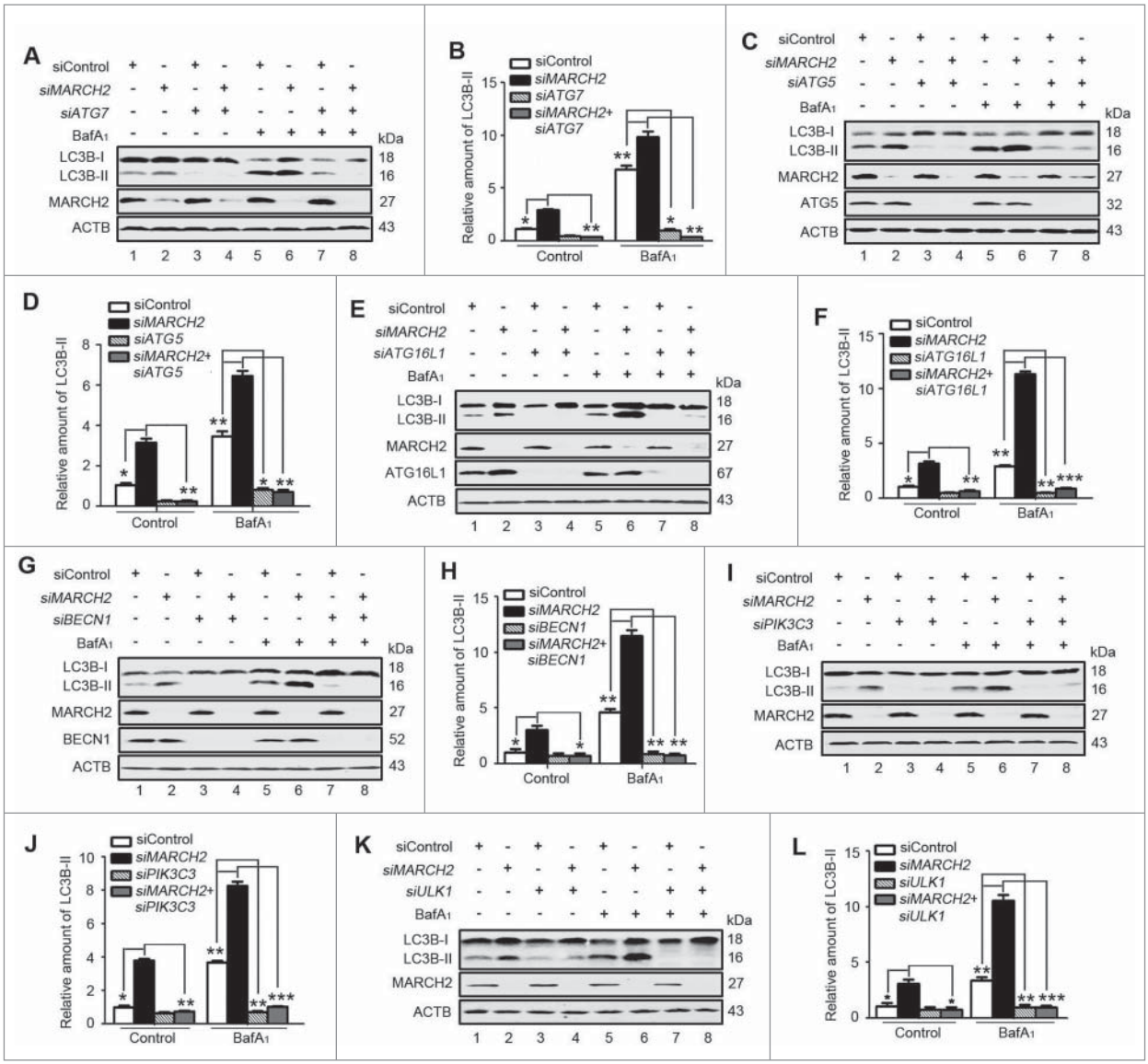

Figure 3. *MARCH2* silencing-mediated autophagy is associated with ULK1 and the BECN1-PIK3C3 complex. (A, C, E, G, I, K) Hela cells were transfected with the indicated siRNAs for 48 h and then treated with or without BafA1 (10 nM) for the last 6 h. The levels of endogenous LC3B-II were detected by western blotting. (B, D, F, H, J, L) Quantification of amounts of LC3B-II relative to ACTB in cells treated as in (A, C, E, G, I, K). Average value in *siControl*-transfected cells without $BafA_1$ treatment was normalized as 1. Data are means ± SD of results from 3 experiments. *, $P < 0.05$; **, $P < 0.01$; ***, $P < 0.001$.

increased (Fig. 4A). Taken together, these results suggested that ablation of *MARCH2* leads to inactivation of the PIK3CA-AKT axis, which could result in activation of TSC2 and the subsequent inactivation of MTOR signals.

Additionally, other signaling pathways were also measured. As shown in Figure 4B and C, *MARCH2* ablation had no significant influence on the phosphorylation of MAPK8/JNK1-MAPK9/JNK2-MAPK109/JNK3, MAPK1/ERK2-MAPK3/ERK1, MAPK/p38 and PRKAA1/2 (AMPK α1 and α2). Conversely, phosphorylation of RPS6KB1 kinase was increased in MARCH2-overexpressing cells (Fig. 4D), which indicated that MARCH2 overexpression promoted MTOR signaling.

The following experiments were used to further demonstrate whether inhibition of MTOR signaling is a necessary for MARCH2-regulated autophagy. A constitutively active form of $RHEB^{Q64L}$, which stimulates the phosphorylation of RPS6KB1 and EIF4EBP1 through activation of MTOR signaling, was transfected into HeLa cells to recover MTOR activity. As shown in Figure 4E and F, the phosphorylation level of RPS6KB1 was upregulated in $RHEB^{Q64L}$ overexpressing cells, indicating that the activity of MTOR was restored in *MARCH2* knockdown cells. Simultaneously, overexpression of $RHEB^{Q64L}$ eliminated the SQSTM1 degradation and LC3B lipidation induced by *siMARCH2* (Fig. 4E, lane 4 vs. lane 2). The increased free GFP in *siMARCH2*-treated GFP-LC3B HeLa cells was also reversed (Fig. 4G and H, lane 4 vs. lane 2). Conversely, overexpression of an inactive form of $RHEB^{D60K}$ failed to reverse the activity of MTOR and the level of autophagy (Fig. 4E–H, lane 6 vs. lane 2).

The impact of MTOR regulation on MARCH2 activity has been examined under autophagy-inducing conditions. Rapamycin (RAPA), a conventional inducer of autophagy by inhibiting MTOR activity was used in our studies. In normal condition, the phosphorylation levels of RPS6KB1 were decreased in si*MARCH2*-treated cells (Fig. 4A, lane 2 vs. lane 1; Fig. S6A and B, lane 2 vs.

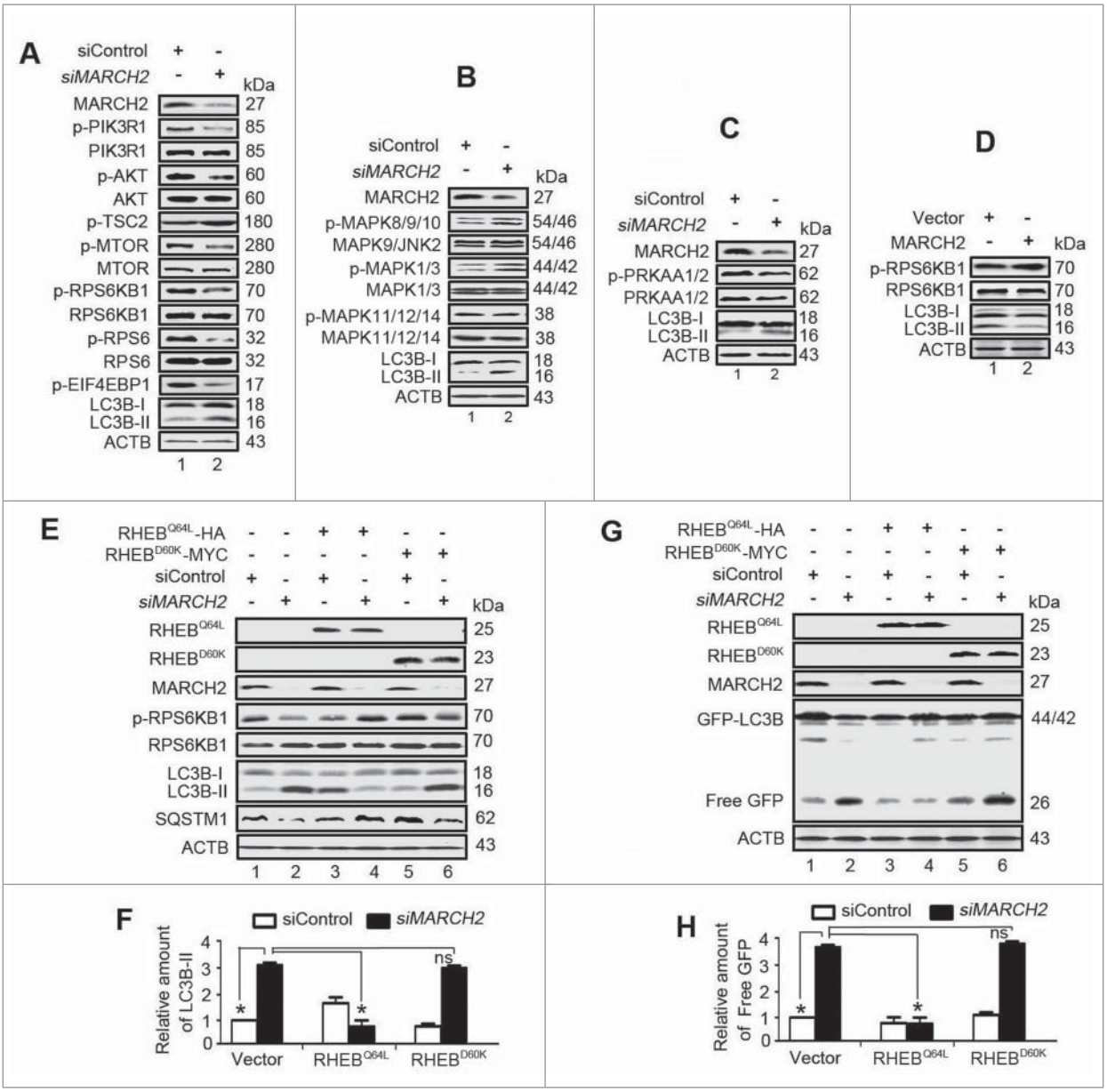

Figure 4. PIK3CA-AKT-MTOR signaling is involved with *MARCH2*-ablation-triggered autophagy. (A) Western blotting analysis of total and phosphorylation levels of PIK3R1/p85 (Tyr458), AKT (Ser473), TSC2 (Thr1462), MTOR (Ser2448), RPS6KB1 (Thr389), RPS6 (Ser235/236) and EIF4EBP1 (Thr37/6) in 293T cells transfected with *siControl* or *siMARCH2* for 48 h. (B and C) Western blotting analysis of total and phosphorylation levels of MAPK8/9/10 (Thr183/Tyr185), MAPK1/3 (Thr202/Tyr204), MAPK/p38 (Thr180/Tyr182) and PRKAA1/2 (Thr172) in 293T cells transfected with *siControl* or *siMARCH2* for 48 h. (D) Western blotting analysis of total and phosphorylation levels of RPS6KB1 (Thr389) in 293T cells transfected with Vector or MARCH2 plasmid for 24 h. (E) HeLa cells were first treated with *siControl or siMARCH2* for 24 h, then transfected with vectors expressing constitutively active (Q64L) or inactive (D60K) RHEB mutants for 24 h. Cell extracts were analyzed by western blotting as indicated. (F) Quantification of amounts of LC3B-II relative to ACTB in cells treated as in (E). Average value in *siControl*-transfected alone cells was normalized as 1. Data are means ± SD of results from 3 experiments. (G) Stable GFP-LC3B-HeLa cells were first treated with *siControl or siMARCH2* for 24 h, then transfected with vectors expressing constitutively active (Q64L) or inactive (D60K) RHEB mutants for 24 h. Cell extracts were analyzed by western blotting as indicated. (H) Quantification of amounts of free GFP relative to ACTB in cells treated as in (G). Average value in *siControl*-transfected alone cells was normalized as 1. Data are means ± SD of results from 3 experiments. *, $P < 0.05$; ns, not significant.

lane 1) and increased in MARCH2-overexpressed cells (Fig. 4D, lane 2 vs. lane 1; Fig. S6A and B, lane 4 vs. lane 3). After rapamycin treatment, the levels of phosphorylated (p)-RPS6KB1 was further decreased or disappeared in *MARCH2* knockdown cells, but the LC3B-II accumulation was further enhanced in such condition (Fig. S6A and B, lane 6 vs. lane 2). Simultanously, rapamycin could attenuate the increased p-RPS6KB1 and partially restore LC3B lipidation in MARCH2-overexpressed cells (Fig. S6A and B, lane 8 vs. lane 4). In other words, MARCH overexpression could resist the reduction of p-RPS6KB and the increase of LC3B lipidation in rapamycin-treated cells (Fig. S6A and B, lane 8 vs. lane 7), and *MARCH2* knockdown accelerate this phenotype (Fig. S6A and B, lane 6 vs. lane5), supporting that MTOR signaling is involved with MARCH2-regulated autophagy under control and autophagy-inducing condition.

MARCH2 associates with CFTR via the PDZ domain

Previous studies indicated that CFTR functions as a chloride channel and controls the regulation of other transport

pathways.[30,31] Defective CFTR induces aggresome formation and lung inflammation in cystic fibrosis through reactive oxygen species (ROS)-TG2-BECN1-mediated autophagy inhibition.[32,33] CFTR is a substrate of MARCH2. Based on these observations, the hypothesis was proposed that MARCH2 regulates autophagy via CFTR. To further confirm the correlation of MARCH2, CFTR and autophagy, a series of plasmids of encoding MARCH2 and CFTR were constructed and tested (Fig. 5A)

HA-MARCH2 and other indicated plasmids were cotransfected into 293T cells. Twenty-four h later, the cell lysates were subjected to immunoprecipitation (IP). Immunoblotting showed that MARCH2 coprecipitated with wild-type CFTR ($CFTR^{WT}$) (Fig. 5B), while MARCH2 failed to coprecipitate with $CFTR^{F508\Delta}$ (Fig. 5B). Further assay uncovered that the loss of the RING domain of MARCH2 did not prevent the interaction between MARCH2 and $CFTR^{WT}$ (Fig. 5C), whereas loss of the PDZ domain of MARCH2 ablated binding to $CFTR^{WT}$ (Fig. 5D). Reciprocally, HA-MARCH2 was detected in the $CFTR^{WT}$ immunoprecipitates (Fig. 5E), but not in those of $CFTR^{PDZ\Delta}$ (Fig. 5F), which indicated that the PDZ domain is required for the interaction between CFTR and MARCH2.

The interaction between CFTR and MARCH2 could also be observed by an affinity isolation approach. As shown in Figure 5G–I, the GST-MARCH2 fusion protein or GST-$MARCH2^{RING\Delta}$ could precipitate $CFTR^{WT}$ from cell lysates, but GST-$MARCH2^{PDZ\Delta}$ was inactive. These results suggested that MARCH2 binds to CFTR in a PDZ domain-dependent manner.

To assess whether MARCH2 is directly associated with CFTR, we introduced the RTS wheat germ continuous exchange cell-free (CECF) translation system. Recombinant GST, GST-MARCH2 or GST-MARCH2 mutants were mixed with CFTR protein obtained from wheat-germ lysate and performed an affinity isolation assay. Results showed that MARCH2 is directly associated with CFTR via PDZ domain (Fig. S7C). These data were consistent with those shown in Figure 5G–I.

Cheng et al.[34] report the ubiquitination and degradation of CFTR by MARCH2 through its association with adaptor proteins GOPC/CAL and STX6. We further investigated whether the interaction of CFTR and MARCH2 depends on GOPC and STX6. The effective siRNAs of *GOPC* and *STX6* were screened (Fig. S7A and B). The results from GST affinity isolation assay showed that knockdown of *GOPC* or *STX6* had no significant influence on the association of MARCH2 and CFTR (Fig. S7D). Furthermore, knockdown of *GOPC* or *STX6* had no obvious impact on the accumulation of LC3B-II induced by

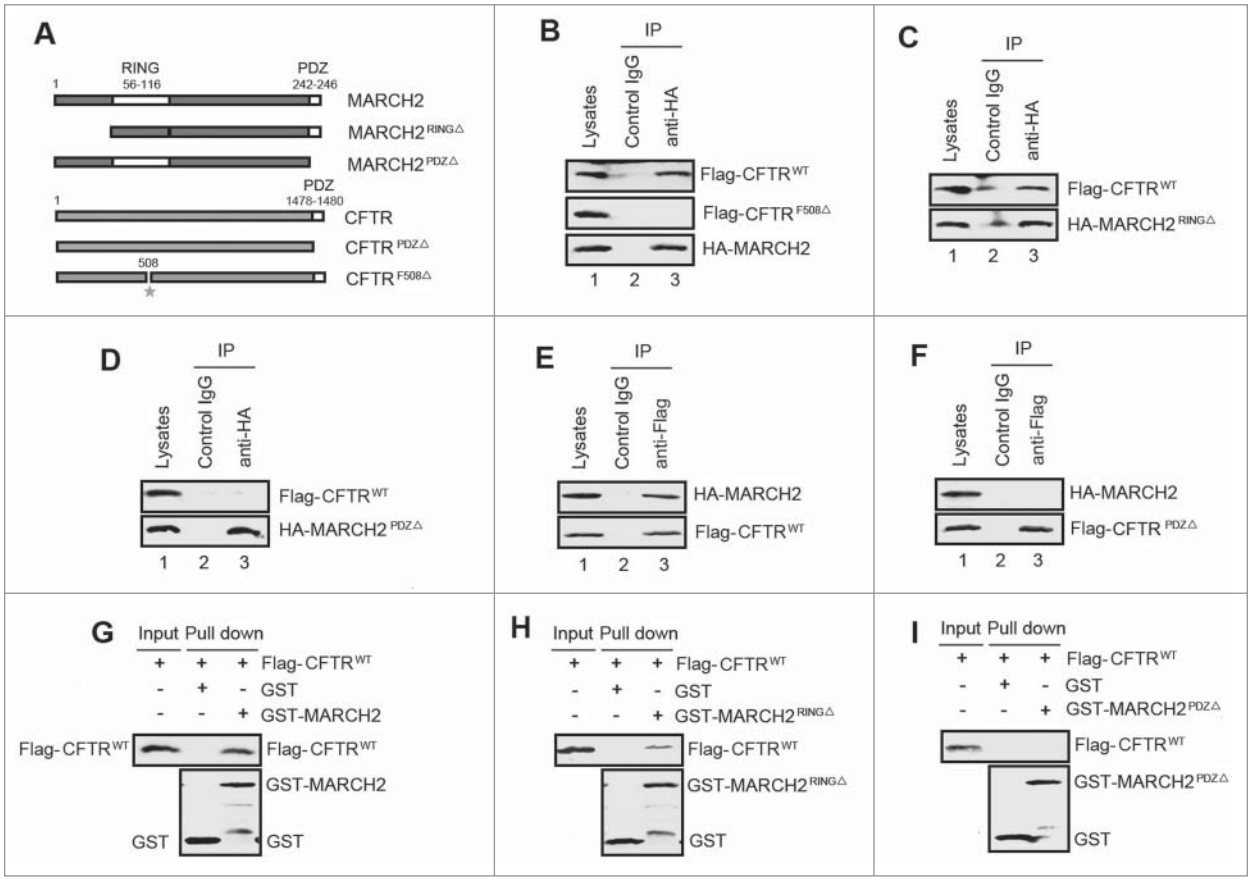

Figure 5. MARCH2 associates with CFTR via the PDZ domain. (A) Truncation mutants including $MARCH2^{RING\Delta}$, $MARCH2^{PDZ\Delta}$, $CFTR^{PDZ\Delta}$ and $CFTR^{F508\Delta}$ were constructed. (B) 293T cells were cotransfected with HA-MARCH2 and FLAG-$CFTR^{WT}$ or FLAG-$CFTR^{F508\Delta}$ for 24 h. Total cell extracts were subjected to IP using either an anti-HA or a isotype control IgG. HA and FLAG were detected in the immunoprecipitates by western blotting. (C and D) 293T cells were cotransfected with FLAG-$CFTR^{WT}$ and HA-$MARCH2^{RING\Delta}$ or HA-$MARCH2^{PDZ\Delta}$ for 24 h. Total cell extracts were subjected to IP using either an anti-HA or a control IgG. HA and FLAG were detected in the immunoprecipitates by western blot. (E and F) 293T cells were cotransfected with HA-MARCH2 and FLAG-$CFTR^{WT}$ or FLAG-$CFTR^{PDZ\Delta}$ for 24 h. Total cell extracts were subjected to IP using either an anti-FLAG or a control IgG. HA and FLAG were detected in the immunoprecipitates by western blotting. (G to I) GST protein and GST-MARCH2 (G) or GST-$MARCH2^{RING\Delta}$ (H) or GST-$MARCH2^{PDZ\Delta}$ (I) fusion protein immobilized on Glutathione-Sepharose beads were incubated with FLAG-$CFTR^{WT}$-transfected HEK293 cell lysates at 4°C for 4 h. CFTR and GST were detected in the washed beads by western blotting.

siMARCH2 (Fig. S7E), indicating that MARCH2-regulated autophagy at least in part, involved with the activity of CFTR, little relationship with GOPC and STX6.

CFTR positively regulates cell autophagy in tumor cells

Accumulating evidence suggests that CFTR plays a key role in the progression and metastasis of cancer. CFTR may be a tumor suppressor or promoter, according to the type of tumor.[35-40] At present, the relationship between CFTR and autophagy in tumor cells remains unclear. So we next investigated whether CFTR regulates conventional autophagy in tumor cells. Repeated experiments showed that the levels of CFTR were downregulated in rapamycin-treated HeLa cells, and the decreased CFTR could be recovered using E64d plus pepstatin A or MG132, indicating that CFTR degradation involves both proteasome and autophagy pathways (Fig. S8A). In CFTR-overexpressing HeLa cells, the levels of endogenous LC3B-II were enhanced, with or without $BafA_1$, compared with the vector control (Fig. 6A and B, lane 2 vs. lane 1, lane 4 vs. lane 3). CFTR also significantly increased RAPA-induced LC3B lipidation (Fig. 6A, lane 6 vs. lane 5, lane 8 vs. lane 7). Similar results were obtained in A549 cells (Fig. S9A and B). $CFTR^{F508\Delta}$ overexpression had no obvious influence on cell autophagy (Fig. S8B). The results hinted that CFTR promoted autophagosome formation both in normal and stress states in HeLa and A549 cells.

Experiments were then performed in *CFTR* knockdown cells. An effective siRNA against *CFTR* (*siCFTR*-3) was validated at the mRNA and protein levels by RT-PCR and western blotting, respectively (Fig. S8C and D). Compared with the *sicontrol, siCFTR-3* reduced the level of endogenous LC3B-II in HeLa cells, with or without $BafA_1$ (Fig. 6C and D, lane 2 vs. lane 1, lane 4 vs. lane 3). Decreased ATG12–ATG5 was also observed in *siCFTR*-treated cells (Fig. 6C, lane 2 vs. lane 1, lane 4 vs. lane 3). Additionally, knockdown of *CFTR* significantly attenuated RAPA-induced LC3B conversion, with or without $BafA_1$ (Fig. 6E and F, lane 4 vs. lane 3, lane 6 vs. lane 5). Similar results were observed in A549 cells (Fig. S9C and D). In accordance with the results of western blotting, *CFTR* ablation reduced the number of GFP-LC3B puncta per cell in the presence or absence of $BafA_1$ (Fig. 6G and H). The RAPA-induced GFP-LC3B dots were also reduced under such conditions (Fig. 6G and H). Taken together, the results suggested that *CFTR* deficiency impaired the autophagosome formation, under normal and stress conditions.

We then investigated the autophagic flux. As shown in Figure 6I and J, a weaker free GFP band was observed in *CFTR*-silenced GFP-LC3B HeLa cells than control cells (Fig. 6I, lane 2 vs. lane 1). The degradation of exogenous polyQ80 aggregates was blocked in *CFTR* knockdown cells (Fig. 6K). By contrast, CFTR overexpression promoted polyQ80 clearance, revealing that *CFTR* knockdown impairs autophagic substrate clearance. The specific effects of *CFTR* deficiency were assessed using a rescue experiment. As shown in Figure 6L and M, the *siCFTR*-induced decreased LC3B conversion was upregulated in cells transfected with the CFTR plasmid (Fig. 6L, lane 3 vs. lane 2), but not by expression of $CFTR^{F508\Delta}$(Fig. 6L, lane 4 vs. lane 2). Collectively, knockdown of *CFTR* attenuated autophagosome synthesis and impaired the clearance of autophagic substrates, while $CFTR^{F508\Delta}$ overexpression had no obvious influence on cell autophagy.

MARCH2 *promotes the ubquitination and degradation of CFTR, and inhibits CFTR-BECN1 signaling*

Because MARCH2 is an E3-ubiquitin ligase of CFTR, we investigated whether MARCH2 negatively regulates autophagy by promoting the ubquitination and degradation of CFTR. We first analyzed the effect of MARCH2 on the stability of CFTR. As shown in Figure 7A and B, lane 2 vs. lane 1, MARCH2 overexpression reduced the levels of endogenous CFTR, while *MARCH2* deficiency had no obvious influence on CFTR levels (Fig. 7A, lane 4 vs. lane 3). Further investigation showed that $MARCH2^{RING\Delta}$ overexpression prevented CFTR degradation (Fig. 7C and D, lane 3 vs. lane 1), while $MARCH2^{PDZ\Delta}$ overexpression failed to affect the degradation of CFTR (Fig. 7C, lane 4 vs. lane 1), indicating that the RING domain is required for MARCH2-mediated degradation of CFTR. We then tested the influence of MARCH2 on the half-life of CFTR. A chase assay using the translation inhibitor cycloheximide (CHX, 100 μg/ml) revealed that overexpression of MARCH2 sped up the degradation of CFTR in a time-dependent manner (Fig. 7E and F), while *MARCH2* silencing delayed the degradation of CFTR (Fig. S10A, lane 13 to 16), implying that the half-life of CFTR is shorter in MARCH2-overexpressing HeLa cells. Similar findings were acquired by immunofluorescence analysis. As shown in Fig. S10B, overexpression of MARCH2 accelerated the fluorescence quenching of CFTR both in cytoplasm and plasma membrane, while MARCH2 silencing delayed this phenotype. These results suggested that MARCH2 may regulate the instability of the CFTR protein.

Protein ubiquitination is associated with the destabilization and degradation of proteins. Thus, the ubiquitination levels of CFTR were measured after cotransfection with the indicated plasmids in HeLa cells. Immunoprecipitation and western blotting showed that CFTR ubiquitination levels were elevated with increased expression of MARCH2 (Fig. 7G), while *MARCH2* silencing had no obvious effect on CFTR ubiquitination levels (Fig. 7G). Our data suggested that MARCH2 mediated the ubquitination and degradation of CFTR.

We further investigated the significance of the interaction between MARCH2 and CFTR. As shown in Figure 8A and B, *MARCH2* silencing increased the accumulation of LC3B-II, with or without of $BafA_1$. By contrast, *CFTR* deficiency significantly decreased LC3B-II accumulation in *MARCH2*-silenced HeLa cells, with or without $BafA_1$ (Fig. 8A and B, lane 4 vs. lane 2, lane 8 vs. lane 6). Similar results were found in A549 cells (Fig. S9E and F). Confocal microscopy data revealed that the increased GFP-LC3B puncta induced by *siMARCH2* were inhibited after treatment with *siCFTR* (Fig. 8C and D). In *siMARCH2*-treated GFP-LC3B HeLa cells, increased free GFP was observed compared with siControl-treated cells (Fig. 8E and F, lane 2 vs. lane 1). However, cotransfection of *siMARCH2* and *siCFTR* reduced the accumulation of free GFP compared with *siMARCH2* alone (Fig. 8E, lane 4 vs. lane 2), which indicated that autophagic flux was impaired by CFTR inhibition. Collectively, these data indicated that knockdown of *CFTR*

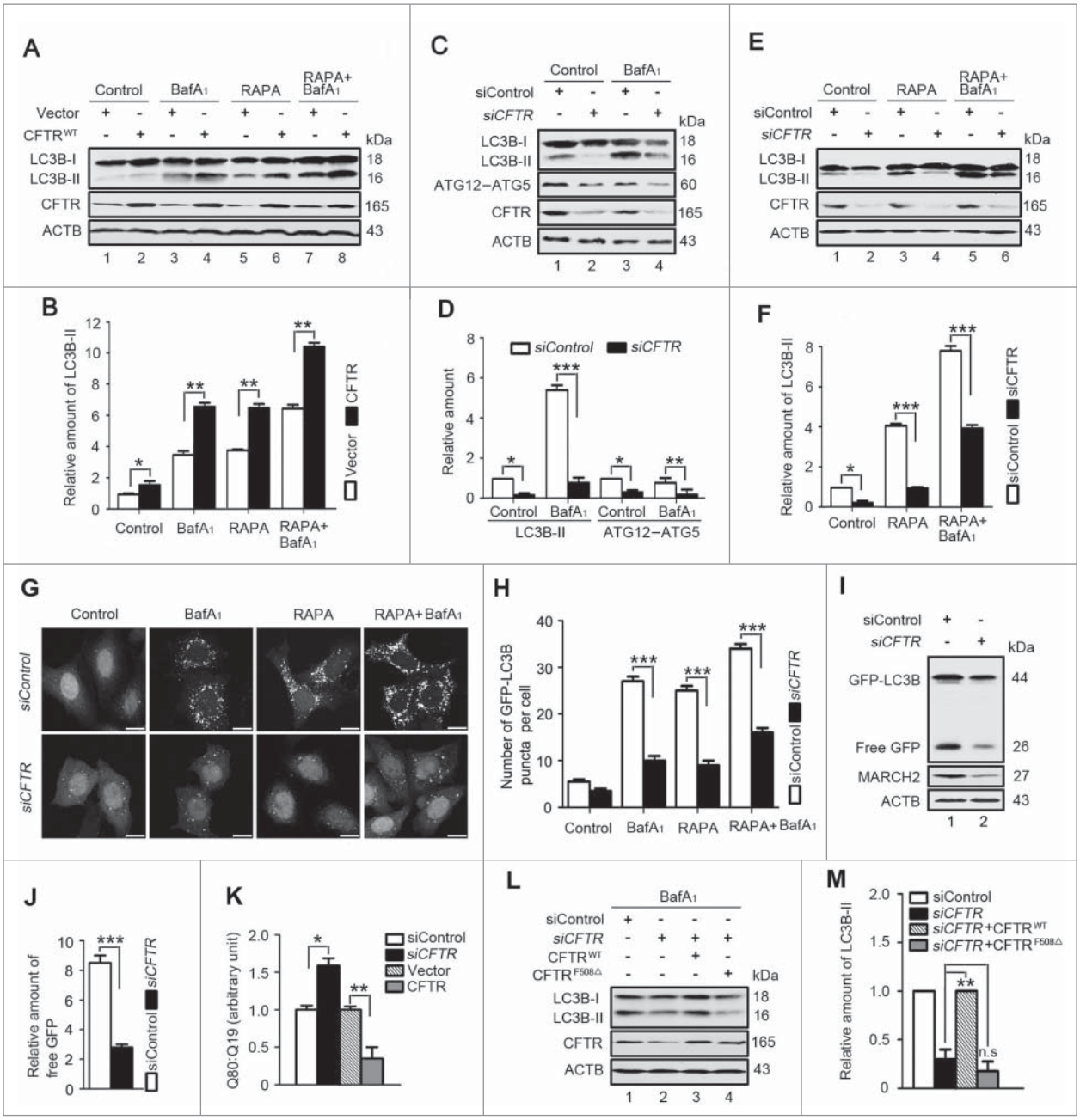

Figure 6. CFTR positively regulates cell autophagy. (A) HeLa cells were transfected with vector or $CFTR^{WT}$-encoding plasmid for 24 h, and treated with or without $BafA_1$ (10 nM) and/or rapamycin (5 μM) for the last 6 h. The levels of LC3B-II were detected by western blotting. (B) Quantification of LC3B-II levels relative to ACTB in cells treated as in (A). Average value in vector-transfected cells without $BafA_1$ or rapamycin treatment was normalized as 1. Data are means ± SD of results from 3 experiments. (C) Western blotting analysis of endogenous LC3B-II and ATG12–ATG5 levels in HeLa cells transfected with *siControl* or *siCFTR* for 48 h and treated with or without $BafA_1$ (10 nM) for the last 6 h. (D) Quantification of amounts of LC3B-II relative to ACTB in cells treated as in (C). Average value in *siControl*-transfected cells without $BafA_1$ treatment was normalized as 1. Data are means ± SD of results from 3 experiments. (E) Western blotting analysis of endogenous LC3B-II levels in HeLa cells transfected with siControl or siCFTR for 48 h, and treated with or without $BafA_1$ (10 nM) and/or rapamycin (5 μM) for the last 6 h. (F) Quantification of amounts of LC3B-II relative to ACTB in cells treated as in (E). Average value in *siControl*-transfected cells without $BafA_1$ or rapamycin treatment was normalized as 1. Data are means ± SD of results from 3 experiments. (G) The treatment of GFP-LC3B-stably transfected Hela cells was as same as in (A), the distribution GFP-LC3B was observed by confocal microscopy. Scale bar: 25 μm. (H) Quantification of GFP-LC3B puncta per cell treated as in (G). Data are means ± SD of at least 50 cells scored. (I) HeLa cells stably expressing GFP-LC3B were cotransfected with *siControl* or *siCFTR* for 48 h. Levels of free GFP were analyzed by western blotting. (J) Quantification of amounts of free GFP protein relative to ACTB in cells treated as in (I). The average value in *siControl*-transfected cells was normalized as 1. Data are means ± SD of results from 3 experiments. (K) HeLa cells were cotransfected with polyQ80-luciferase (or polyQ19-luciferase) and the indicated siRNAs for 48 h or the indicated plasmid for 24 h. PolyQ80-luciferase: polyQ19-luciferase ratios were analyzed using the Dual Luciferase Reporter System. The average value in *siControl*-transfected or vector-transfected cells was normalized as 1. Data are means ± SD of results from 3 experiments. (L) HeLa cells were transfected with *siControl* or *siCFTR* alone, and together with the $CFTR^{WT}$- or $CFTR^{F508\Delta}$-encoding plasmids for 48 h, and then treated with $BafA_1$ (10 nM) for the last 6 h. The levels of LC3B-II were tested by western blotting. (M) Quantification of LC3B-II levels relative to ACTB in cells treated as in (L). Average value in vector-transfected cells without $BafA_1$ treatment was normalized as 1. Data are means ± SD of results from 3 experiments. *, $P < 0.05$; **, $P < 0.01$; ***, $P < 0.001$; ns, not significant.

attenuated the autpophagy induced by *siMARCH2*. On the other hand, MARCH2 overexpression blocked the lipidation of LC3B induced by CFTR (Fig. 8G and H, lane 3 vs. lane 2, lane 7 vs. lane 6), while *siMARCH2* augmented the accumulation of LC3B-II caused by CFTR in U2OS cells with or without $BafA_1$ treatment (Fig. 8G, lane 4 vs. lane 2, lane 8 vs. lane 6). These

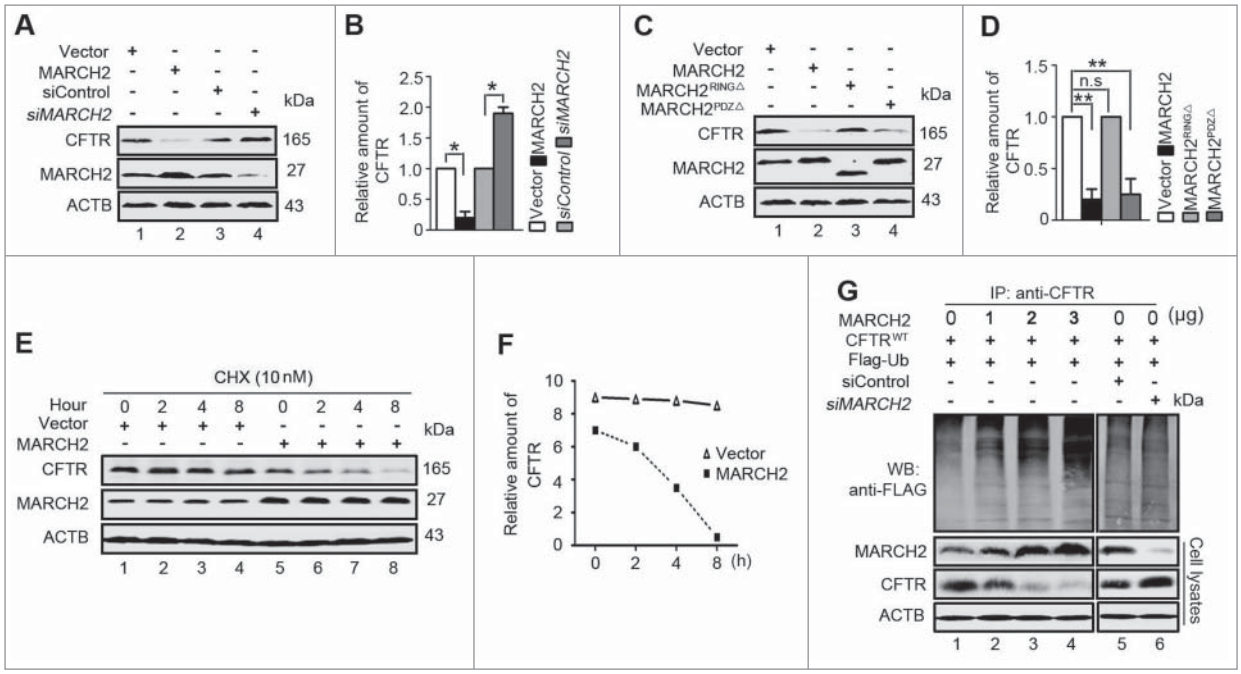

Figure 7. MARCH2 promotes ubquitination and degradation of CFTR. (A and C) HeLa cells were transfected with *siControl*, *siMARCH2*, Vector, MARCH, MARCH2-$^{RING\Delta}$ or MARCH2$^{PDZ\Delta}$ plasmids for 48 h, respectively. The levels of endogenous CFTR were examined by western blotting. (B and D) Quantification of CFTR levels relative to ACTB in cells treated as in (A and C). Average value in vector- or *siControl*-transfected cells was normalized as 1. Data are means ± SD of results from 3 experiments. *, $P < 0.05$; **, $P < 0.01$; ns, not significant. (E) HeLa cells were transfected with vector or MARCH2 plasmid for 24 h, and treated with cycloheximide (CHX, 10 nM) for the indicated time, respectively. The levels of endogenous CFTR were measured by western blotting. (F) Quantification of CFTR levels relative to ACTB in cells treated as in (E). (G) 293T cells were cotransfected with the indicated plasmids for 24 h or siRNA against *MARCH2* for 48 h. The cells lysates were then immunoprecipitated with an anti-CFTR antibody and probed with an anti-FLAG antibody.

results suggested that CFTR-mediated autophagy signaling is inactivated by MARCH2 overexpression and promoted by MARCH2 silencing. Taken together, our results implied that the MARCH2 and CFTR are mutually antagonistic in the regulation of cellular autophagy.

It was reported that *CFTR* inactivation induces BECN1 downregulation and defective autophagy through the ROS-TG2-BECN1 pathway.[32,33] Therefore, we next investigated the effects of MARCH2 on CFTR signaling. As shown in Figure 8I andJ, the levels of BECN1 protein were elevated in *MARCH2*-depleted cells (Fig. 8I, lane 2 vs. lane 1), but decreased in *siCFTR*-treated cells (Fig. 8I, lane 3 vs. lane 1). Simultaneously, cotransfection of *siMARCH2* and *siCFTR* attenuated BECN1 expression compared with *siMARCH2* alone (Fig. 8I, lane 4 vs. lane 2). On the other hand, a strong BECN1 band was observed in CFTR overexpressing cells (Fig. 8I, lane 6 vs. lane 5). When cells were cotransfected with MARCH2 and CFTR plasmids, the expression of BECN1 was downregulated (Fig. 8I, lane 7 vs. lane 6), while *MARCH2* knockdown had the opposite effect (Fig. 8I, lane 8 vs. lane 6). Linked with the results from Fig. 3G, which demonstrated that *BECN1* silencing inhibited the autophagy induced by *siMARCH2*, these data suggested that MARCH2 negatively regulates autophagy, at least partly via CFTR-BECN1 signaling.

Knockout of MARCH2 *inhibits xenograft tumor growth*

The xenograft tumor model was performed using BALB/c nude mice to provide functional evidence on the role of MARCH2 in autophagy. Control (wild-type) HCT116 cells and *MARCH2* KO HCT116 cells were subcutaneously injected in the right axilla of BALB/c nude mice. At 20 d after inoculation, mice were sacrificed and the tumor of each mouse was separated and photographed. As shown in Fig. S11A, the tumor size of the *MARCH2* KO group was smaller than that in control group, indicating that knockout of *MARCH2* in HCT116 cells results in an inhibition of tumorigenicity. Data from immunoblotting suggested that the decreased levels of SQSTM1 were observed in tumor tissues of mice inoculated with *MARCH2* KO HCT116 cells, compared with those of control group (Fig. S11B), indicating the occurrence of autophagy. These data suggested that *MARCH2*-depletion mediated autophagy could exert antitumor activities in vivo on HCT116 cells.

Discussion

In the present study, for the first time, we proposed that MARCH2 is involved in the regulation of autophagy. Our data showed that MARCH2 overexpression inhibited basal or stress-induced autophagy, whereas knockdown or knockout of *MARCH2* in tumor cells displayed higher levels of autophagy than that control cells. In vivo experiments demonstrate that *MARCH2* knockout mediated autophagy could exert antitumor activities.

Autophagy is a multistage process. Many key ATG molecules and important complexes, such as the ULK1 complex, the PIK3C3-BECN1 complex, the ATG12-ATG5-ATG16L1 complex and LC3B (a mammalian ortholog of yeast Atg8) is involved in this process.[1,2] To determine at which step autophagy is influenced by MARCH2, several essential *ATG* genes were silenced and used to determine the effects on MARCH2-mediated autophagy. The results revealed that the deficiencies

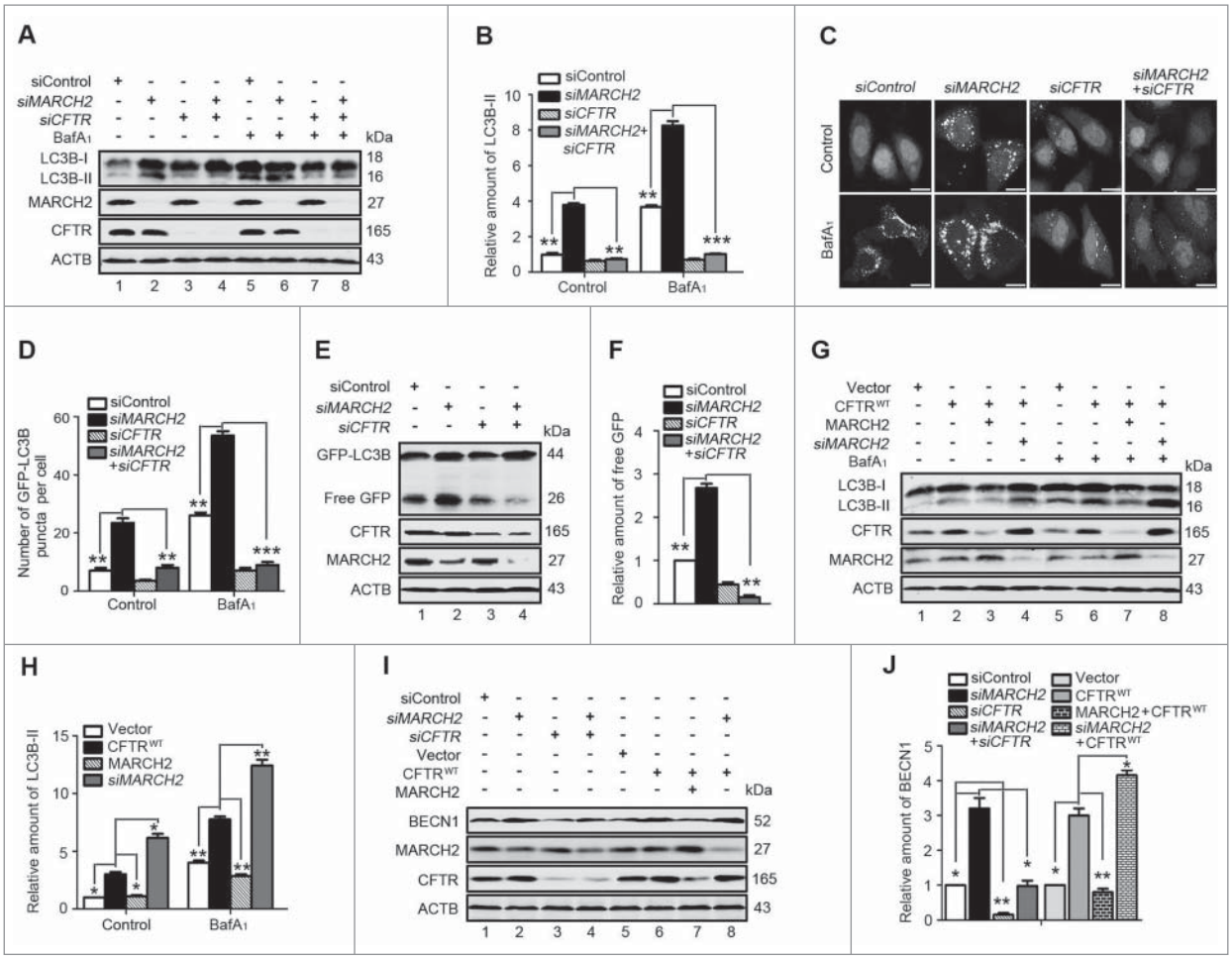

Figure 8. MARCH2 and CFTR are mutually antagonistic in the regulation of autophagy. (A) Western blotting analysis of endogenous LC3B-II levels in HeLa cells transfected with the indicated *siRNAs* for 48 h, and then treated with or without $BafA_1$ (10 nM) for the last 6 h. (B) Quantification of LC3B-II levels relative to ACTB in cells treated as in (A). Average value in *siControl*-transfected cells without $BafA_1$ treatment was normalized as 1. Data are means ± SD of results from 3 experiments. (C) Representative confocal microscopy images of GFP-LC3B distribution in stably transfected GFP-LC3B HeLa cells treated as in (A). Scale bar: 25 μm. (D) Quantification of GFP- LC3B puncta per cell treated with reagents as indicated in (C). Data are means ± SD of at least 50 cells scored. (E) Western blotting analysis of free GFP levels in stably transfected GFP-LC3B Hela cells also transfected with the indicated *siRNA* for 48 h. (F) Quantification of free GFP levels relative to ACTB in cells treated as in (E). Average value in *siControl*-transfected cells was normalized as 1. Data are means ± SD of results from 3 experiments. (G) Western blotting analysis of endogenous LC3B-II levels in HeLa cells transfected with the indicated plasmids or *siRNAs* for 48 h, and then treated with or without $BafA_1$ (10 nM) for the last 6 h. (H) Quantification of LC3B-II levels relative to ACTB in cells treated as in (G). Average value in *siControl*-transfected cells without $BafA_1$ treatment was normalized as 1. Data are means ± SD of results from 3 experiments. (I) Western blotting analysis of BECN1 levels in 293T cells transfected with the indicated plasmids or *siRNAs* for 48 h. (J) Quantification of BECN1 levels relative to ACTB in cells treated as in (I). Average value in vector- or *siControl*-transfected cells was normalized as 1. Data are means ± SD of results from 3 experiments. $^{*}P < 0.05$; $^{**}P < 0.01$; $^{***}P < 0.001$.

of *ATG7, ATG5, ATG16L1, BECN1, PIK3C3* and *ULK1* attenuated the level of autophagy induced by *MARCH2* depletion, which demonstrated that MARCH2 might act on the upstream portion of the autophagic pathway.

The MTOR signaling pathway plays a critical role in the regulation of autophagy. Here, we found that the phosphorylation levels of MTOR, RPS6KB1, EIF4EBP1 and RPS6 were decreased in *MARCH2*-silenced cells. Consistent with this finding, the kinase activity of PIK3CA and AKT (upstream of MTOR) also decreased in *MARCH2*-depleted cells (Fig. 4A), which was accompanied by an increase in p-TSC2 levels. Therefore, the PIK3CA-AKT signal negatively regulates TSC1/2, and inactivates MTOR, which consequently induces autophagy. Importantly, when cells were transfected with $RHEB^{Q64L}$, a constitutive active form of RHEB that activates the protein kinase activity of MTOR and stimulates the phosphorylation of RP6KB1 and EIF4EBP1, *MARCH2* deficiency-induced autophagy was prevented. However, $RHEB^{Q64L}$, the inactive form of RHEB had no such effects. We also detected other signaling, such as PRKAA1/2 and MAPK (Fig. 4B and C). However, there were no obvious changes in these signals in *MARCH2*-silenced cells. Our studies proved that MARCH2 regulates autophagy through the PIK3CA-AKT-MTOR pathway.

MARCH2 exerts its biological activities through its interacting partner. MARCH2 interacts with STX6 (syntaxin 6) as a regulator of trafficking between the TGN and early or recycling endosomes.[11] The interaction between MARCH2 and DLG1 resulted in DLG1 ubiquitination, suggesting that MARCH2 might be a molecular bridge linking endocytic tumor suppressor molecules (e.g. syntaxins) to the polarity-deciding scaffold protein DLG1.[12] MARCH2 functions as an E3 ubiquitin ligase, promoting endocytosis and lysosomal degradation of carvedilol-bound ADRB2/β2AR, mediating the beneficial effects in treating heart failure patients with carvedilol.[13] CFTR (cystic fibrosis transmembrane conductance regulator) is also a

specific substrate of MARCH2. By connecting with the GOPC-STX6-CFTR complex, MARCH2 advances the ubiquitination and degradation of CFTR.[14] In our study, using CO-IP and GST affinity isolation assays, the interaction between MARCH2 and CFTR was also demonstrated. MARCH2 interacts with CFTR via the PDZ domain to regulate autophagy. Importantly, this interaction is independent on the GOPC and STX6 in our experimental system. Furthermore, knockdown of *GOPC or STX6* had no obvious influence on cell autophagy induced by *MARCH2* knockdown.

Data from our experiments indicated that overexpression of MARCH2 impaired autophagosome formation induced by CFTR, while *MARCH2* knockdown enhanced this effect. Furthermore, we found that MARCH2 overexpression increased ubiquitination and degradation of CFTR in a RING-dependent manner, illustrating that MARCH2 negatively regulates autophagy by destabilizing CFTR. Conversely, depletion of CFTR attenuated *MARCH2* knockdown-induced autophagy, implying that the interaction between MARCH2 and CFTR was mutually antagonistic in the regulation of cellular autophagy.

CFTR is a plasma membrane cAMP-regulated Cl^- channel that is responsible for transepithelial salt and fluid transport.[31] Loss-of-function mutations in the CFTR gene can cause the lethal recessive genetic disorder, cystic fibrosis (CF).[41] The majority of CF patients have the F508 deletion mutation ($CFTR^{F508\Delta}$).[42] This mutant causes autophagy deficiency, leading to the accumulation of protein aggregates, lung inflammation and, ultimately, CF. In $Cftr^{F508\Delta}$ transgenic homozygous mice, defective autophagy can be restored by BECN1 overexpression,[43] indicating that BECN1 plays an important role in CFTR-mediated autophagy.

Accumulating evidence indicates that the intracellular levels of ROS are increased in CF, resulting from defective CFTR function, which leads to the upregulation of TG2 protein levels and sustained TG2 activation. The persistently high TG2 protein levels might lead to crosslinking, increased ubiquitination and functional sequestration of its substrates, such as BECN1. This would impair autophagosome formation and drive defective autophagy. In our studies, knockdown *CFTR* or *MARCH2* overexpression promoted the production of ROS (data not shown) and decreased the level of BECN1 (Fig. 8I and J). BECN1 is essential for *MARCH2* depletion-induced autophagy; therefore, we deduced that MARCH2 negatively regulates autophagy by inactivating CFTR, stimulating TG2 activity and promoting degradation of BECN1 by upregulating ROS levels. On this point, further research is needed in the future.

$CFTR^{F508\Delta}$ is closely related with CF disease. This mutant is a temperature-sensitive allele that is unable to fold correctly at physiological temperature. It is recognized by the ER quality control system and degraded by the proteasome. It is not transmitted from ER to Golgi apparatus and plasma membrane.[41,42] In our study, MARCH2 is not associated with $CFTR^{F508\Delta}$, and $CFTR^{F508\Delta}$ had no obvious effect on autophagy in tumor cell lines. This result is different from previous studies in CF airway epithelial cells,[32,42,43] which might be explained by the different cell lines and culture conditions used.

Accumulating evidence suggests that CFTR plays a key role in the progression and metastasis of cancer. Genetic variations in CFTR may be associated with increased or decreased risk for developing cancers,[44-46] suggesting that CFTR is a tumor suppressor or promoter, according to the type of tumor. The high level of CFTR expression is associated with tumor malignancy, progression in ovarian cancer and cervical cancer.[35,36] In non-small-cell lung cancer and breast cancer, CFTR is significantly downregulated and low expression of CFTR is significantly correlated with progression and metastasis of cancers.[37,38] Sun et al.[39] report that disrupted interaction between CFTR and AF-6/afadin aggravates malignant phenotypes of colon cancer. In prostate cancer, CFTR suppresses tumor progression through *MIR193B* targeting PLAU (plasminogen activator, urokinase). As far as we known, the relationship between CFTR and autophagy in tumor cells remains unclear. Our studies demonstrate that CFTR plays a positive role in regulating conventional autophagy in tumor cells. It was known that autophagy has both pro- and antitumor effects in tumor biology. The relationship among CFTR, autophagy and tumors is worthy of further investigation.

In summary, our study revealed a novel role for MARCH2 as a negative regulator of cell autophagy. This effect involves the inhibition of PIK3CA-AKT-MTOR and CFTR signal pathways. Further study is required to clarify the correlation among MARCH, CFTR and CF or tumor in patients. Similarly, the physical and functional connection between the MARCH2 and CFTR in different conditions will be also elucidated in the further experiments.

Materials and methods

Antibodies and reagents

Polyclonal antibodies were as follows: MARCH2 (Abcam, AB76397), anti-LC3B (Sigma-Aldrich, L7543), CFTR (Santa Cruz Biotechnology, sc-8909), anti-ACTB/β-actin (Tianjin Sungene, KM9001), anti-GST (Tianjin Sungene, KM8005), anti-FLAG (Tianjin Sungene, KM8002L), anti-HA (Tianjin Sungene, KM8004), anti-GFP (Tianjin Sungene, KM8009L), anti-CTSB/cathepsin B (Abcam, AB33538), anti-CTSD/cathepsin D (Abcam, AB6313), anti-ATG16L1 (MBL, PM040), Anti-BECN1/beclin1 (MBL, PD017). The following antibodies were purchased from Cell Signaling Technology: anti-SQSTM1/p62 (5114), anti-ubiquitin (3936), anti-ATG5 (12994S), anti-MTOR (2983S), anti-phospho-MTOR (Ser2448; 2971S), anti-RPS6KB1 (2708S), anti-phospho-RPS6KB1 (Thr389; 9234S), anti-RPS6 (2217S), anti-phospho-RPS6 (Ser235/236; 4858S), anti-PIK3R1/p85 (4292), anti-phospho-PIK3R1/p85 (Tyr458; 4228S), anti-AKT (9272S), anti-phospho-AKT (Ser473; 4060S), anti-phospho-EIF4EBP1 (Thr37/46; 2855S), anti-phospho-TSC2 (Thr1462; 3617S), anti-MAPK1/p42-MAPK3/p44 (4695S), anti-phospho-MAPK1/p42-MAPK3/p44 (Thr202/Tyr204; 4370S), anti-MAPK9/JNK2 (9258S), anti-phospho-MAPK8/JNK1-MAPK9/JNK2-MAPK10/JNK3 (SAPK/JNK Thr183/Tyr185; 9255S), anti-MAPK11-MAPK12-MAPK14 (8690S), anti-phospho-MAPK/p38 (Thr180/Tyr182; 4511S), anti-PRKAA1/2 (AMPK, α1 and α2; 2532S), anti-phospho-PRKAA1/2 (Thr172; 2535S). Secondary antibodies included DyLight 800/DyLight 680-conjugated IgG against mouse (Rockland, 610-145-002/610-144-002) or rabbit (Rockland, 611-145-002/611-144-002) and FITC/RBITC-conjugated IgG against

mouse (Bioss Inc., bs-0296GFITC/bs-0296G-RBITC) or rabbit (Bioss Inc., bs-0295G-FITC/bs-0295G-RBITC). Other reagents used in this study were: Dual-Luciferase ®Reporter (DLR™) Assay System (Promega, E1910), bafilomycin A_1 ($BafA_1$; Sigma-Aldrich, B1793), DQ-BSA (Life Technologies, D12051), 3-methyladenine (Sigma-Aldrich, M9281), wortmannin (Sigma-Aldrich, W1628), LY294002 (Cayman Chemical, 70920), E64d (ENZO Life Sciences, ALX-260-007-M005), pepstatin A (Sigma-Aldrich, P5318-5MG), cycloheximide (Calbiochem, 239763), MG132 (Sigma-Aldrich, C2211), Hoechst 33342 (Sigma-Aldrich, 14533), LysoTracker Red (Life Technologies, L7528), Rapamycin (Sigma-Aldrich, R117) and RIPA Lysis Buffer (50 mM Tris-HCl, pH 7.4, 150 mM NaCl, 1% NP-40; Beyotime, P0013D).

Plasmid construction and siRNA

The *MARCH2* cDNA was amplified from HeLa cells by PCR using the forward primer (5′-CCGGAATTCATGACGACGG GTGACTGC-3′) and reverse primer (5′-CGCGGATCCCG-TACTGGTGTCTCCTCTGCCA-3′). The insert was released by EcoR I and Hind III then subcloned into the EcoRI site of pcDNA.3.1/myc-His(−)B (Life Technologies, V85520) to construct the pcDB-MARCH2 plasmid, abbreviated as MARCH2 in this study. Based on this plasmid, we constructed the following plasmids in succession: MARCH2-MYC, HA-MARCH2, HA-$MARCH2^{RING\Delta}$, HA-$MARCH2^{PDZ\Delta}$, GST-MARCH2, GST- $MARCH2^{RING\Delta}$ and GST- $MARCH2^{PDZ\Delta}$ (Fig. 5A). pcDNA3-wtCFTR and pcDNA3-$CFTR^{F508\Delta}$ plasmids were kindly provided by Dr. Chunying Li (Wayne State University School of Medicine, USA). Based on the pcDNA3-wt-CFTR plasmid, we constructed the pcDNA3-$CFTR^{PDZ\Delta}$ construct (Fig. 5A). All constructs were confirmed by DNA sequencing. The mTagRFP-mWasabi-LC3B plasmid was kindly provided by Jian Lin (Peking University, Beijing, China). The polyQ80-luciferase and polyQ19-luciferase plasmids were kindly provided by Conrad C. Weihl (Washington University School of Medicine, USA). The GFP-LC3B plasmid and was kindly provided by Zhenyu Yue (Mount Sinai School of Medicine, New York, USA). GFP-WIPI2 plasmid was gift from Dr. Tassula Proikas-Cezanne (Eberhard Karls University Tuebingen, Germany), GFP-ATG16L1 plasmid was gift from Dr. Noboru Mizushima (The University of Tokyo, Japan), GFP-STX17 plasmid was provided by Dr. Hong Zhang (Chinese Academy of Sciences, China). MYC-$RHEB^{Q64L}$ and MYC-$RHEB^{D60K}$ were provided by Weiguo Zhu (Peking University Health Science Center, Beijing, China). The siRNAs against the indicated genes used in this study were listed in Table 1.

Table 1. The sequence of siRNAs used in this study.

siRNAs	sequence
MARCH2 siRNA	5′-GUGCUACCUUGCUUGAGAATT-3′
CFTR siRNA-1	5′-GCAGAUGACAUUCUCGACAUCUCUATT-3′
CFTR siRNA-2	5′-CCGGCUCAUCCAGAUGGCCUACGAATT-3′
CFTR siRNA-3	5′-CCGGCUCAUCCAGAUGGCCUACGAATT-3′
GOPC siRNA-1	5′-CCAAGCGGACAUCACUUAUTT-3′
GOPC siRNA-2	5′-GCUGACUCUGGUACCAUUATT-3′
GOPC siRNA-3	5′-CCUGCUCAUGAUAAGCUUUTT-3′
STX6 siRNA-1	5′-GUGCAGGCAUUAGCUGAAATT-3′
STX6 siRNA-2	5′-CACUGGAACAACAGAUAAATT-3′
STX6 siRNA-3	5′-GAAGAUUUCUCUCACGAAUTT-3′
ATG7 siRNA	5′-CAGUGGAUCUAAAUCUCAAACUGAU-3′
ATG5 siRNA	5′-GCAACUCUGGAUGGGAUUG-3′
ATG16L1 siRNA	5′-CCCGUGAUGACUUGCUAAA-3′
BECN1 siRNA	5′-GCUGCCGUUAUACUGUUCU-3′
PIK3C3 siRNA	5′-GUGUGAUGAUAAGGAAUAU-3′
ULK1 siRNA	5′-UGGUCAUGGAGUAUUGUAATT-3′
Control siRNA	5′-UUCUCCGAACGUGUCACGU-3′

Cell culture, transfections and treatments

HeLa, U2OS, A549, HCT116 and 293T cell lines were cultured in DMEM (Invitrogen, 12800-017) supplemented with 10% fetal bovine serum and maintained at 37°C in a humidified chamber with 5% CO_2. The stably transfected GFP-LC3B HeLa cell line was a gift from Li Yu (Tsinghua University Beijing, China). Cells were transfected with plasmids using MegaTran 1.0 Transfection Reagent (OriGene, TT200004), according to the manufacturer's instruction, while siRNA transfection was performed using Lipofectamine 2000 reagent (Life Technologies, 11668-019). Cell autophagy was induced using the MTOR inhibitor rapamycin (RAPA, 5 μM). Inhibition of autophagy was achieved by treating cells with 10 nM of $BafA_1$, which blocks the fusion of autophagosomes and lysosomes, or with 10 mM of 3-MA, 10 μM of wortmannin, or 10 μM of LY294002 (blockers of the early stage of autophagy).

Poly Q degradation assay

Cells were cotransfected with polyQ80-luciferase or control polyQ19-luciferase and the indicated plasmids using MegaTran 1.0 Transfection Reagent, according to the manufacturer's protocol. After treatment at the desired time, cell lysates prepared from polyQ80-luciferase or polyQ19-luciferase transfected cells were dispensed in triplicate into a 96-well assay plate (COSTAR, Corning Inc., 3925) containing 100 mL of Luciferase Assay Buffer II (containing the luciferase assay substrate) from the DLRTM Assay System, according to the manufacturer's protocol. The assay plate was mixed by pipetting 2 or 3 times, and the stabilized luminescent signal was measured by a Veritas Microplate Luminometer (Turner Biosystems, Sunnyvale, CA, USA). Data were expressed as the ratio of polyQ80-luciferase: polyQ19-luciferase luminescence signal values in each group, as described previously.[47] All samples were assayed in triplicate, and the results were shown from 3 independent experiments.

Knockout of the MARCH2 gene by CRISPR-Cas9–mediated genome editing

MARCH2 knockout cell line by CRISPR-Cas9-mediated genome editing was established in HCT116 cells. Target sequences for CRISPR interference were designed by Shanghai Biomodel Organism Science & Technology Development Co., Ltd (China). The target sequences for human *MARCH2* are TCCAAGGTCGTGGAGGCTACGGG (Exon 2). The *MARCH2* DNA was amplified by PCR using the forward primer (5′-AGA TGG TGC AAA CTG AGG CT-3′) and reverse primer (5′-AAC TAG CCA GGT GTG GTG AC-3′). Sequence analysis revealed that the mutation (TCGTGG→C) resulted in frameshifts with premature termination by introducing stop codon,

removal of translation initiation codon and deletion of functional domain such as RING domain and PDZ domain of MARCH2.

Immunofluorescence, fluorescence, and confocal microscopy

Cells were cultured in confocal dishes and treated as indicated, fixed with 4% paraformaldehyde and permeabilized with 0.2% Triton X-100 (Beyotime, ST795). The dishes were then incubated with fetal bovine serum overnight and exposed to primary antibodies for 1 h at 4°C. After washing 3 times with phosphate-buffered saline (137 mM NaCl, 2.7 mM KCl, 10 mM Na_2HPO_4, 2 mM KH_2PO_4, pH 7.4; Solarbio, P1010), the dishes were covered with FITC/RBITC-conjugated secondary antibody solution. Nuclei were stained with Hoechst 33342. Morphological alterations in the cells were observed and documented using an Olympus FluoViewTM FV1000 Confocal Microscope (Olympus, Melville, NY, USA). The number of GFP-LC3B or endogenous LC3B puncta per cell was assessed in 50 cells, and statistical data were obtained from 3 independent experiments.

Transmission electron microscopy

Treated HeLa cells were initially fixed in 0.1 M sodium phosphate buffer containing 3% glutaraldehyde (pH 7.4) and then fixed in 0.1 M sodium phosphate buffer containing 1% OsO_4 (pH 7.2) for 2 h at 4°C. The cells were dehydrated in a graded series of ethanol. Cells were embedded in Ultracut (LEICA ULTRACUT R, Bensheim, Germany) and sliced into 60-nm sections. Ultrathin sections were stained with uranyl acetate and lead citrate, and observed under a JEM-1230 transmission electron microscope (JEOL-USA, Inc., Peabody, MA, USA).

Flow cytometry

HeLa cells were cotransfected with a plasmid expressing mTagRFP-mWasabi-LC3 and *Control* siRNA or *MARCH2* siRNA, at a ratio of 1:3 for 48 h, then cultured in EBSS for 4 h. The cells were then harvested and resuspended in ice-cold PBS. mTagRFP and mWasabi fluorescent signals were analyzed on a FACS Calibur flow cytometer (Becton Dickinson, USA). The percentage of $mTagRFP^{high}$ $mWasabi^{low}$ cells was assessed from 3 independent experiments.

Immunoprecipitation and western blot analysis

For the IP analysis, treated cells were collected and disrupted in IP lysis buffer (300 mM NaCl, 50 mM Tris, pH 8.0, 0.4% NP-40 [Beyotime, ST366], 10 mM $MgCl_2$, 2.5 mM $CaCl_2$) containing protease inhibitors (Roche Diagnostics, 04693116001). Total cell extracts (1 mg per sample) were mixed with precleared protein G Sepharose™ Fast Flow (GE Healthcare, 17-0618-01) and appropriate antibodies, followed by incubation for 4 h at 4°C. The beads were collected by centrifugation, washed 5 times using washing buffer (50 mM Tris, pH 8.0, 150 mM NaCl, 0.4% NP-40, and 5 mM $MgCl_2$), resuspended in 2 × SDS loading buffer and then subjected to western blotting as described previously.[16] The protein bands were visualized using DyLight 800/DyLight 680-conjugated secondary antibodies, and the infrared fluorescence image was obtained using an Odyssey infrared imaging system (LI-CORBiosciences, Lincoln, NE, USA).

GST affinity isolation assay

Recombinant GST, GST-MARCH2 or GST-MARCH2 mutants were expressed in *Escherichia coli* strain BL21 (DE3) and purified. Equal amounts of these proteins immobilized on glutathione-Sepharose TM 4B (GE Healthcare, 17-0756-01) were incubated with whole cell lysates extracted from transfected 293T cells or Flag-CFTR protein obtained from wheat germ lysate (RTS™100 wheat germ CECF kit; biotechrabbit GmbH, 2402100) at 4°C for 4 h. The beads were then washed and resuspended in 2 × SDS loading buffer and analyzed by western blot.[16]

Tumorigenicity in nude mice

A nude mouse xenograft model was established using 6- to 8-wk-old female BALB/c nude mice (Experimental Animal Center, Peking University Health Sciences Center, Beijing, China). Mice were housed and maintained in a pathogen-free facility, and all experimental procedures and protocols were approved by the Institutional Authority for Laboratory Animal Care of Peking University. Control (wild-type) HCT116 cells or *MARCH2* KO HCT116 cells were subcutaneously injected in the right axilla of BALB/c nude mice in a total volume of 100 μl (4×10^6 cells). At 20 d after inoculation, the mice were killed; and the tumor of each mouse was separated and photographed. One part of tumor tissues was homogenized and protein was extracted for immunoblotting with anti-SQSTM1, anti-LC3 or anti-ACTB.

Statistical analysis

Data are presented as the mean ± SD. Differences between groups were analyzed using the Student *t* test for continuous variables. Statistical significance in this study was set at $P < 0.05$. All analyses were performed using GraphPad Prism 5.

Abbreviations

3-MA	3-methyladenine
AKT	v-akt murine thymoma viral oncogene homolog
ATG	autophagy-related
$BafA_1$	bafilomycin A_1
BECN1	Beclin 1 autophagy related
CTSB	cathepsin B
CTSD	cathepsin D
CF	cystic fibrosis
CFTR	cystic fibrosis transmembrane conductance regulator
CHX	cycloheximide
EBSS	Earle's balanced salt solution
EIF4EBP1	eukaryotic translation initiation factor 4E binding protein 1

GOPC/CAL	golgi-associated PDZ and coiled-coil motif containing
IP	immunoprecipitation
KO	knockout
MAP1LC3B/LC3B	microtubule-associated protein 1 light chain 3 β
MAPK	mitogen-activated protein kinases
MARCH2	membrane associated ring-CH-type finger 2
MTOR	mechanistic target of rapamycin (serine/threonine kinase)
PDZ	PSD-95/Discs large/ZO-1 homologous
PIK3C3	phosphatidylinositol 3-kinase catalytic subunit type 3
PIK3CA	phosphatidylinositol-4,5-bisphosphate 3-kinase catalytic subunit α
PIK3R1	phosphoinositide-3-kinase regulatory subunit 1
PRKAA	protein kinase AMP-activated catalytic subunit α
RAPA	rapamycin
RPS6	ribosomal protein S6
RPS6KB1	ribosomal protein S6 kinase B1
SQSTM1	sequestosome 1
STX6	syntaxin 6
TEM	transmission electron microscopy
TSC	tuberous sclerosis complex

Disclosure of potential conflicts of interest

No potential conflicts of interest were disclosed.

Acknowledgments

The authors thank Drs. Noboru Mizushima, Conrad C. Weihl, Tassula Proikas-Cezanne, Zhenyu Yue, Chunying Li, Hong Zhang, Li Yu, Weiguo Zhu, Jian Lin for providing valuable plasmids for this study; Yali Ren and Ming Cheng for technical help in transmission electron microscopy.

Funding

This work was supported by a grant from the National Key Basic Research Program of China (973, 2011CB910103) and the National Natural Science Foundation of China (91430101, 81420108002).

References

[1] Levine B, Klionsky DJ. Development by self-digestion: molecular mechanisms and biological functions of autophagy. Dev Cell 2004; 6:463-77; PMID:15068787; http://dx.doi.org/10.1016/S1534-5807(04)00099-1

[2] Mizushima N, Levine B, Cuervo AM, Klionsky DJ. Autophagy fights disease through cellular self-digestion. Nature 2008; 451:1069-75; PMID:18305538; http://dx.doi.org/10.1038/nature06639

[3] Hanada T, Noda NN, Satomi Y, Ichimura Y, Fujioka Y, Takao T, Inagaki F, Ohsumi Y. The Atg12-Atg5 conjugate has a novel E3-like activity for protein lipidation in autophagy. J Biol Chem 2007; 282:37298-302; PMID:17986448; http://dx.doi.org/10.1074/jbc.C700195200

[4] Kabeya Y, Mizushima N, Ueno T, Yamamoto A, Kirisako T, Noda T, Kominami E, Ohsumi Y, Yoshimori T. LC3, a mammalian homologue of yeast Apg8p, is localized in autophagosome membranes after processing. Embo J 2000; 19:5720-8; PMID:11060023; http://dx.doi.org/10.1093/emboj/19.21.5720

[5] Mizushima N, Yoshimori T. How to interpret LC3 immunoblotting. Autophagy 2007; 3:542-5; PMID:17611390; http://dx.doi.org/10.4161/auto.4600

[6] Rubinsztein DC, Cuervo AM, Ravikumar B, Sarkar S, Korolchuk V, Kaushik S, Klionsky DJ. In search of an "autophagomometer". Autophagy 2009; 5:585-9; PMID:19411822; http://dx.doi.org/10.4161/auto.5.5.8823

[7] Mizushima N, Yoshimori T, Levine B. Methods in mammalian autophagy research. Cell 2010; 140:313-26; PMID:20144757; http://dx.doi.org/10.1016/j.cell.2010.01.028

[8] Klionsky DJ, Abdalla FC, Abeliovich H, Abraham RT, Acevedo-Arozena A, Adeli K, Agholme L, Agnello M, Agostinis P, Aguirre-Ghiso JA, et al. Guidelines for the use and interpretation of assays for monitoring autophagy. Autophagy 2012; 8:445-544; PMID:22966490; http://dx.doi.org/10.4161/auto.19496

[9] Bartee E, Mansouri M, Hovey NB, Gouveia K, Fruh K. Downregulation of major histocompatibility complex class I by human ubiquitin ligases related to viral immune evasion proteins. J Virol 2004; 78:1109-20; PMID:14722266; http://dx.doi.org/10.1128/JVI.78.3.1109-1120.2004

[10] Boutell C, Sadis S, Everett RD. Herpes simplex virus type 1 immediate-early protein ICP0 and is isolated RING finger domain act as ubiquitin E3 ligases in vitro. J Virol 2002; 76:841-50; PMID:11752173; http://dx.doi.org/10.1128/JVI.76.2.841-850.2002

[11] Nakamura N, Fukuda H, Kato A, Hirose S. MARCH-II is a syntaxin-6-binding protein involved in endosomal trafficking. Mol Biol Cell 2005; 16:1696-710; PMID:15689499; http://dx.doi.org/10.1091/mbc.E04-03-0216

[12] Cao Z, Huett A, Kuballa P, Giallourakis C, Xavier RJ. DLG1 is an anchor for the E3 ligase MARCH2 at sites of cell-cell contact. Cell signal 2008; 20:73-82; PMID:17980554; http://dx.doi.org/10.1016/j.cellsig.2007.08.019

[13] Han SO, Xiao K, Kim J, Wu JH, Wisler JW, Nakamura N, Freedman NJ, Shenoy SK. MARCH2 promotes endocytosis and lysosomal sorting of carvedilol-bound beta(2)-adrenergic receptors. J Cell BIOL 2012; 199:817-30; PMID:23166351; http://dx.doi.org/10.1083/jcb.201208192

[14] Cheng J, Guggino W. Ubiquitination and degradation of CFTR by the E3 ubiquitin ligase MARCH2 through its association with adaptor proteins CAL and STX6. Plos ONE 2013; 8:e68001; PMID:23818989; http://dx.doi.org/10.1371/journal.pone.0068001

[15] He P, Peng Z, Luo Y, Wang L, Yu P, Deng W, An Y, Shi T, Ma D. High-throughput functional screening for autophagy-related genes and identification of TM9SF1 as an autophagosome-inducing gene. Autophagy 2009; 5:52-60; PMID:19029833; http://dx.doi.org/10.4161/auto.5.1.7247

[16] Li Y, Zhao Y, Hu J, Xiao J, Qu L, Wang Z, Ma D, Chen Y. A novel ER-localized transmembrane protein, EMC6, interacts with RAB5A and regulates cell autophagy. Autophagy 2013; 9:150-63; PMID:23182941; http://dx.doi.org/10.4161/auto.22742

[17] Zhao Y, Hu J, Miao G, Qu L, Wang Z, Li G, Lv P, Ma D, Chen Y. Transmembrane protein 208: a novel ER localized protein that regulates autophagy and ER stress. PLoS One 2013; 8:e64228; PMID:23691174; http://dx.doi.org/10.1371/journal.pone.0064228

[18] Wang Z, Hu J, Li G, Qu L, He Q, Lou Y, Song Q, Ma D, Chen Y. PHF23 (plant homeodomain finger protein 23) negatively regulates cell autophagy by promoting ubiquitination and degradation of E3 ligase LRSAM1. Autophagy 2014; 10:2158-70; PMID:25484098; http://dx.doi.org/10.4161/auto.36439

[19] Ravikumar B, Duden R, Rubinsztein DC. Aggregate prone proteins with polyglutamine and polyalanine expansions are degraded by autophagy. Hum Mol Genet 2002; 11:1107-17; PMID:11978769; http://dx.doi.org/10.1093/hmg/11.9.1107

[20] Hsu PD, Lander ES, Zhang F. Development and applications of CRISPR-Cas9 for genome engineering. Cell 2014; 157(6):1262-78; PMID:24906146; http://dx.doi.org/10.1016/j.cell.2014.05.010

[21] Sugita S, Ito K, Yamashiro Y, Moriya S, Che XF, Yokoyama T, Hiramoto M, Miyazawa K. EGFR-independent autophagy induction with gefitinib and enhancement of its cytotoxic effect by targeting autophagy with clarithromycin in non-small cell lung cancer cells. Biochem Biophys Res Commun 2015; 461(1):28-34; PMID:25858318; http://dx.doi.org/10.1016/j.bbrc.2015.03.162

[22] Dooley HC, Wilson MI, Tooze SA. WIPI2B links PtdIns3P to LC3 lipidation through binding ATG16L1. Autophagy 2015; 11(1):190-1; PMID:25629784

[23] Polson HE, de Lartigue J, Rigden DJ, Reedijk M, Urbé S, Clague MJ, Tooze SA. Mammalian Atg18 (WIPI2) localizes to omegasome-anchored phagophores and positively regulates LC3 lipidation. Autophagy 2010; 6(4):506-22; PMID:20505359; http://dx.doi.org/10.4161/auto.6.4.11863

[24] Dooley HC, Razi M, Polson HE, Girardin SE, Wilson MI, Tooze SA. WIPI2 links LC3 conjugation with PI3P, autophagosome formation, and pathogen clearance by recruiting Atg12-5-16L1. Mol Cell 2014; 55(2):238-52; PMID:24954904; http://dx.doi.org/10.1016/j.molcel.2014.05.021

[25] Hegedűs K, Takáts S, Kovács AL, Juhász G. Evolutionarily conserved role and physiological relevance of a STX17/Syx17 (syntaxin 17)-containing SNARE complex in autophagosome fusion with endosomes and lysosomes. Autophagy 2013; 9(10):1642-6; PMID:24113031; http://dx.doi.org/10.4161/auto.25684

[26] Itakura E, Kishi-Itakura C, Mizushima N. The hairpin-type tail-anchored SNARE syntaxin 17 targets to autophagosomes for fusion with endosomes/lysosomes. Cell 2012; 151(6):1256-69; PMID:23217709; http://dx.doi.org/10.1016/j.cell.2012.11.001

[27] Zhou C, Zhong W, Zhou J, Sheng F, Fang Z, Wei Y, Chen Y, Deng X, Xia B, Lin J. Monitoring autophagic flux by an improved tandem fluorescent-tagged LC3 (mTagRFP-mWasabi-LC3) reveals that high-dose rapamycin impairs autophagic flux in cancer cells. Autophagy 2012; 8:1215-26; PMID:22647982; http://dx.doi.org/10.4161/auto.20284

[28] Tanida I. Autophagosome formation and molecular mechanism of autophagy. Antioxid Redox Signal 2011; 14:2201-14; PMID:20712405; http://dx.doi.org/10.1089/ars.2010.3482

[29] Surviladze Z, Sterk RT, DeHaro SA, Ozbun MA. Cellular entry of human papillomavirus type 16 involves activation of the phosphatidylinositol 3-kinase/Akt/mTOR pathway and inhibition of autophagy. J Virol 2013; 87:2508-17; PMID:23255786; http://dx.doi.org/10.1128/JVI.02319-12

[30] Pranke IM, Sermet-Gaudelus I. Biosynthesis of cystic fibrosis transmembrane conductance regulator. Int J Biochem Cell Biol 2014; 52:26-38; PMID:24685677; http://dx.doi.org/10.1016/j.biocel.2014.03.020

[31] Li C, Naren AP. CFTR chloride channel in the apical compartments: spatiotemporal coupling to its interacting partners. Integr Biol (Camb) 2010; 2:161-77; PMID:20473396; http://dx.doi.org/10.1039/b924455g

[32] Luciani A, Villella VR, Esposito S, Brunetti-Pierri N, Medina D, Settembre C, Gavina M, Pulze L, Giardino I, Pettoello-Mantovani M, et al. Defective CFTR induces aggresome formation and lung inflammation in cystic fibrosis through ROS-mediated autophagy inhibition. Nat Cell Biol 2010; 12:863-75; PMID:20711182; http://dx.doi.org/10.1038/ncb2090

[33] Luciani A, Villella VR, Esposito S, Brunetti-Pierri N, Medina DL, Settembre C, Gavina M, Raia V, Ballabio A, Maiuri L. Cystic fibrosis: a disorder with defective autophagy. Autophagy 2011; 7:104-6; PMID:21048426; http://dx.doi.org/10.4161/auto.7.1.13987

[34] Cheng J1, Guggino W. Ubiquitination and degradation of CFTR by the E3 ubiquitin ligase MARCH2 through its association with adaptor proteins CAL and STX6. PLoS One 2013; 8(6):e68001; PMID:23818989; http://dx.doi.org/10.1371/journal.pone.0068001

[35] Xu J, Yong M, Li J, Dong X, Yu T, Fu X, Hu L. High level of CFTR expression is associated with tumor aggression and knockdown of CFTR suppresses proliferation of ovarian cancer in vitro and in vivo. Oncol Rep 2015; 33:2227-34; PMID:25738998

[36] Peng X, Wu Z, Yu L, Li J, Xu W, Chan HC, Zhang Y, Hu L. Overexpression of cystic fibrosis transmembrane conductance regulator (CFTR) is associated with human cervical cancer malignancy, progressionand prognosis. Gynecol Oncol 2012; 125:470-6; PMID:22366595; http://dx.doi.org/10.1016/j.ygyno.2012.02.015

[37] Li J, Zhang JT, Jiang X, Shi X, Shen J, Feng F, Chen J, Liu G, He P, Jiang J, et al. The cystic fibrosis transmembrane conductance regulator as a biomarker in non-small cell lung cancer. Int J Oncol 2015; 46:2107-15; PMID:25760446

[38] Zhang JT, Jiang XH, Xie C, Cheng H, Da Dong J, Wang Y, Fok KL, Zhang XH, Sun TT, Tsang LL, et al. Downregulation of CFTR promotes epithelial-to-mesenchymal transitionand is associated with poor prognosis of breast cancer. Biochim Biophys Acta 2013; 1833:2961-9; PMID:23916755; http://dx.doi.org/10.1016/j.bbamcr.2013.07.021

[39] Sun TT, Wang Y, Cheng H, Xiao HZ, Xiang JJ, Zhang JT, Yu SB, Martin TA, Ye L, Tsang LL, et al. Disrupted interaction between CFTR and AF-6/afadin aggravates malignantphenotypes of colon cancer. Biochim Biophys Acta 2014; 1843:618-28; PMID:24373847; http://dx.doi.org/10.1016/j.bbamcr.2013.12.013

[40] Xie C, Jiang XH, Zhang JT, Sun TT, Dong JD, Sanders AJ, Diao RY, Wang Y, Fok KL, Tsang LL, et al. CFTR suppresses tumor progression through miR-193b targetingurokinase plasminogen activator (uPA) in prostate cancer. Oncogene 2013; 32:2282-91; PMID:22797075; http://dx.doi.org/10.1038/onc.2012.251

[41] Gelman MS, Kannegaard ES, Kopito RR. A principal role for the proteasome in endoplasmic reticulum-associated degradation of misfolded intracellular cystic fibrosis transmembrane conductance regulator. J Biol Chem 2002; 277:11709-14; PMID:11812794; http://dx.doi.org/10.1074/jbc.M111958200

[42] Gentzsch M, Chang XB, Cui L, Wu Y, Ozols VV, Choudhury A, Pagano RE, Riordan JR. Endocytic trafficking routes of wild type and DeltaF508 cystic fibrosis transmembrane conductance regulator. Mol Biol Cell 2004; 15:2684-96; PMID:15075371; http://dx.doi.org/10.1091/mbc.E04-03-0176

[43] Luciani A, Villella V R, Esposito S, Gavina M, Russo I, Silano M, Guido S, Pettoello-Mantovani M, Carnuccio R, Scholte B, et al. Targeting autophagy as a novel strategy for facilitating the therapeutic action of potentiators on Delta F508 cystic fibrosis transmembrane conductance regulator. Autophagy 2012; 8:1657-72; PMID:22874563; http://dx.doi.org/10.4161/auto.21483

[44] Padua RA, Warren N, Grimshaw D, Smith M, Lewis C, Whittaker J, Laidler P, Wright P, Douglas-Jones A, Fenaux P, et al. The cystic fibrosis delta F508 gene mutation and cancer. Hum Mutat 1997; 10:45-8; PMID:9222759; http://dx.doi.org/10.1002/(SICI)1098-1004(1997)10:1%3c45::AID-HUMU6%3e3.0.CO;2-L

[45] McWilliams RR, Petersen GM, Rabe KG, Holtegaard LM, Lynch PJ, Bishop MD, Highsmith WE Jr. Cystic fibrosis transmembrane conductance regulator (CFTR) gene mutations and risk for pancreatic adenocarcinoma. Cancer 2010; 116:203-9; PMID:19885835; http://dx.doi.org/10.1002/cncr.25465

[46] Li Y, Sun Z, Wu Y, Babovic-Vuksanovic D, Li Y, Cunningham JM, Pankratz VS, Yang P. Cystic fibrosis transmembrane conductance regulator gene mutation and lung cancer risk. Lung Cancer 2010; 70:14-21; PMID:20116881; http://dx.doi.org/10.1016/j.lungcan.2010.01.005

[47] Ju JS, Miller SE, Jackson E, Cadwell K, Piwnica-Worms D, Weihl CC. Quantitation of selective autophagic protein aggregate degradation in vitro and in vivo using luciferase reporters. Autophagy 2009; 5:511-9; PMID:19305149; http://dx.doi.org/10.4161/auto.5.4.7761